Journal of Advanced Research 46 (2023) 173–188

Contents lists available at ScienceDirect

Journal of Advanced Research

journal homepage: www.elsevier.com/locate/jare

Original Article

Amelioration of type 2 diabetes by the novel 6, 8-guanidyl luteolin quinone-chromium coordination *via* biochemical mechanisms and gut microbiota interaction

Xiaodong Ge [a], Xiaoyu He [g], Junwei Liu [c], Feng Zeng [a], Ligen Chen [c], Wei Xu [c], Rong Shao [c], Ying Huang [a], Mohamed A. Farag [d], Esra Capanoglu [e], Hesham R. El-Seedi [f], Chao Zhao [a,b,*], Bin Liu [a,g,*]

[a] College of Food Science, Fujian Agriculture and Forestry University, Fuzhou, Fujian 350002, China
[b] College of Marine Sciences, Fujian Agriculture and Forestry University, Fuzhou, Fujian 350002, China
[c] College of Marine and Bioengineering, Yancheng Institute of Technology, Yancheng, Jiangsu 224051, China
[d] Pharmacognosy Department, College of Pharmacy, Cairo University, Cairo, Egypt
[e] Department of Food Engineering, Faculty of Chemical and Metallurgical Engineering, Istanbul Technical University, Maslak 34469 Istanbul, Turkey
[f] Pharmacognosy Group, Department of Pharmaceutical Biosciences, BMC, Uppsala University, Uppsala, Box 591, SE 751 24 Uppsala, Sweden
[g] National Engineering Research Center of JUNCAO Technology, Fujian Agriculture and Forestry University, Fuzhou, Fujian 350002, China

HIGHLIGHTS

- Two luteolin derivatives GLQ and GLQ.Cr with hypoglycaemic activity were prepared.
- GLQ.Cr affected the PPAR signaling pathway to improve hyperglycaemia symptoms.
- GLQ.Cr regulation of intestinal microbiota community was verified by fecal microbiota transplantation.

GRAPHICAL ABSTRACT

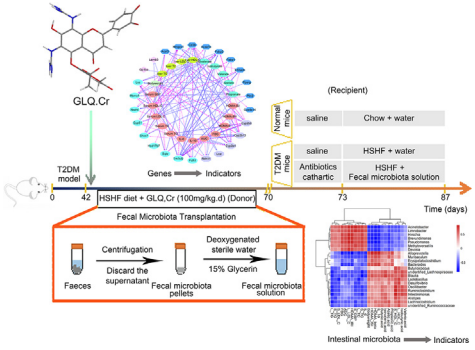

ARTICLE INFO

Article history:
Received 7 January 2022
Revised 17 May 2022
Accepted 8 June 2022
Available online 11 June 2022

ABSTRACT

Introduction: Luteolin is a plant-derived flavonoid that exhibits a broad range of pharmacological activities. Studies on luteolin have mainly focused on its use for hyperlipidaemia prevention, whereas the capacity of the flavonoid to hinder hyperglycaemia development remains underexplored.
Objectives: To probe the anti-hyperglycemic mechanism of 6,8-guanidyl luteolin quinone-chromium

Abbreviations: T2DM, Type 2 diabetes mellitus; FMT, Faecal microbiota transplantation; NAFLD, Non-alcoholic fatty liver disease; HFD, High-fat diets; LUT, Luteolin; MH, Metformin hydrochloride; CrY, Cr-enriched yeast; RNA-seq, RNA sequencing; PPAR, Peroxisome proliferative activated receptor; qPCR, Quantitative PCR; NBS, N-Bromosuccinimide; BPO, Benzoyl peroxide; GLQ, 6,8-guanidyl luteolin quinone; GLQ.Cr, 6,8-guanidyl luteolin quinone-chromium coordination; BrettPhos, 2-(Dicyclohex ylphosphino)-3,6-dimethoxy-2′-4′-6′-tri-i-propyl-1,1′-biphenyl; FT-IR, Fourier transform infrared spectroscopy; HRMS, High resolution mass spectrum; UV–Vis spectrum, Ultraviolet–visible spectroscopy; SEM, Scanning electron microscopy; HSHF, High-sucrose/high-fat; STZ, Streptozotocin; FBG, Fasting blood glucose; OGTT, Oral glucose tolerance test; AUC, Area under the curve; FIN, Fasting insulin; HOMA, Homeostatic model assessment; HOMA-β, HOMA-pancreatic islet β-cell function index; HOMA-IRI, HOMA-insulin resistance index; HOMA-ISI, HOMA-insulin sensitivity index; TC, Total cholesterol; TG, Triacylglycerol; LDL-C, Low-density lipoprotein cholesterol; HDL-C, High-density lipoprotein cholesterol; GSP, Glycated serum protein; Cd36, Fatty acid translocase, cluster of differentiation 36; Fabp, Fabp fatty acid binding protein; Pparg, Peroxisome proliferative activated receptor γ; Cyp4a14, Cytochrome P450 4A14; Scd, Stearoyl-CoA desaturase; SCFAs, Short-chain fatty acids; SD, Standard deviations; BP, Biological process; CC, Cellular component; MF, Molecular function; DEGs, Differentially expressed genes; F/B, Firmicutes to Bacteroidetes; GO, Gene ontology; IL-6, Interleukin-6; IL-10, Interleukin-10.

Peer review under responsibility of Cairo University.

* Corresponding authors at: College of Food Science, Fujian Agriculture and Forestry University, Fuzhou, Fujian 350002, China.
E-mail addresses: mohamed.farag@pharma.cu.edu.eg (M.A. Farag), zhchao@live.cn (C. Zhao), liubin618@hotmail.com (B. Liu).

https://doi.org/10.1016/j.jare.2022.06.003

Keywords:
Anti-hyperglycemic
Luteolin
Intestinal microbiota
Faecal microbiota transplantation
RNA-seq

coordination (GLQ.Cr), and to assess its regulatory effect on intestinal microbiota in type 2 diabetes mellitus (T2DM) mice.

Methods: High-sucrose/high-fat diet-induced and intraperitoneal injection of streptozotocin was used to develop a T2DM model. Glycometabolism related indicators, histopathology, and gut microbiota composition in caecum samples were evaluated, and RNA sequencing (RNA-seq) of liver samples was conducted. Faecal microbiota transplantation (FMT) was further used to verify the anti-hyperglycemic activity of intestinal microbiota.

Results: The administration of GLQ.Cr alleviated hyperglycaemia symptoms by improving liver and pancreatic functions and modulating gut microbe communities (*Lactobacillus, Alistipes*, *Parabacteroides*, *Lachnoclostridium*, and *Desulfovibrio*). RNA-seq analysis showed that GLQ.Cr mainly affected the peroxisome proliferative activated receptor (PPAR) signalling pathway in order to regulate abnormal glucose metabolism. FMT significantly modulated the abundance of *Lactobacillus*, *Alloprevotella*, *Alistipes*, *Bacteroides, Ruminiclostridium, Brevundimonas* and *Pseudomonas* in the caecum to balance blood glucose levels and counteract T2DM mice inflammation.

Conclusion: GLQ.Cr improved the abnormal glucose metabolism in T2DM mice by regulating the PPAR signalling pathway and modulating intestinal microbial composition. FMT can improve the intestinal microecology of the recipient and in turn ameliorate the symptoms of T2DM-induced hyperglycaemia.

Introduction

Over the past 30 years, the diet, physical activity, and habits of humans have changed considerably. Today, high-sucrose/high-fat (HSHF) diet, oily and salty diets, intemperance and irregular eating, sedentary lifestyles, excessive sleep, smoking, alcohol consumption, and other phenomena are increasing, to the detriment of the healthy development of a large proportion of the young and middle-aged populations [1,2]. According to the International Diabetes Federation, the number of adults with diabetes reached ~463 million in 2019 and is expected to increase to 578.4 million by 2030, with the largest number of patients (2019) reported in China (116.4 million), India (77 million), and USA (31 million), respectively. Patients with type 2 diabetes mellitus (T2DM) account for >90% of all diabetes patients and suffer from abnormal oxidative stress and liver tissue damage, which further aggravate T2DM progression and eventually lead to a variety of complications [3]. At present, metformin hydrochloride (MH) is extensively used as a anti-hyperglycemic drug for T2DM. Although it is effective in controlling blood glucose levels, the side effects on the intestinal function of patients should not be overlooked. 5-Hydroxytryptamine was produced when MH was absorbed by the gut. It negatively affected the central nervous system and caused diarrhoea, ultimately impairing intestinal homeostasis [4]. Researchers have reported that natural active ingredients in plants, such as polysaccharides, flavonoids, polypeptides, triterpenes, and so on, regulate the balance of gut microbiota by influencing absorption, transport, metabolism, and other factors in the gut-liver axis, which can alleviate T2DM-related glucose metabolism disorders [5,6]. Zhao et al. reported that the administration of a high-fibre diet alters gut microbiota community and improves serum glucose and lipid level regulation [7]. At present, faecal microbiota transplantation (FMT) has attracted considerable attention as a strategy of promoting the recovery of recipient gut microbiota and homeostasis in the recipient gut-liver axis. The role of the gut-liver axis in metabolic dysfunction and its associated comorbidities i.e., non-alcoholic fatty liver disease (NAFLD) is increasingly recognized and is increasingly a target in drug therapy [8]. De Groot et al. summarized the advantages and disadvantages of FMT techniques, focusing on FMT as a method of metabolic syndrome treatment [9]. Zhou et al. subjected high-fat diets (HFD) mice to FMT to effectively reduce their body weight and NAFLD score [10]. High-glucose and high-fat diets cause disorders in gut microbiota composition, leading to the disruption of the intestinal barrier function and the release of metabolic toxins, and ultimately induce glucose and lipid metabolism disorders [11-13].

Recent studies have shown that the guanidyl functional group regulates intestinal inflammation and anti-hepatoma effects, and allows the correspondingly modified compounds to better penetrate membranes comprising phospholipid bilayer structures, as exemplified by the current use of guanidylation to modify anti-hepatocyte inflammatory drugs [14]. As a microelement, chromium (Cr) is normally found in the urine at levels of 0.2–1.9 μmol/L and participates in glucose metabolism. In particular, Cr(III) deficiency causes insulin resistance and T2DM, while the supplementation of T2DM patients with Cr(III) improves insulin sensitivity and glucose metabolism, in addition to reducing the risk of T2DM-related complications [15]. Ye et al. prepared a sulphated rhamnose polysaccharide-Cr(III) complex and found that it has a satisfactory therapeutic effect on type 2 diabetic mice and can therefore be used as a nutraceutical therapeutic agent for T2DM control [16].

Luteolin (LUT) is a plant-derived bioactive flavonoid with great promise for the treatment of various diseases e.g., hyperlipidaemia and hepatitis. In our previous work, LUT from the ethanolic extract of *Grifola frondosa* was isolated and showed that the compound could improve lipid metabolism [17]. In terms of anti-hyperglycemic effects, few studies have been conducted on LUT. We hypothesized that LUT had poor anti-hyperglycemic effects, and considered LUT as a potential lead compound for structural modification for enhancement of its anti-hyperglycemic activity. Consequently, we herein synthesized 6,8-guanidyl luteolin quinone-chromium coordination (GLQ.Cr) by modifying the structure of LUT with guanidylation and coordination with Cr(III). In addition, LUT, MH and Cr-enriched yeast (CrY) were used as positive controls to investigate the effects of GLQ.Cr on hyperglycemia symptoms in T2DM mice. The anti-hyperglycemic effects of GLQ.Cr on T2DM mice occurred mainly through mediation of the liver peroxisome proliferative activated receptor (PPAR) signalling pathway and regulation of intestinal microbe community structure. To confirm that GLQ.Cr regulates blood glucose levels by modulating intestinal microbe community structure, we also verified the hypoglycaemic effect of the faecal microbiota by liquid transfer from GLQ.Cr-treated T2DM mice (donor) to model T2DM mice (recipient). Such transplant could alleviate T2DM symptoms in the recipient through the modulation of intestinal microbe communities, increasing the abundance of beneficial bacteria, such as *Lactobacillus*, *Alloprevotella*, and *Alistipes*, while decreasing the abundance of

pathogenic bacteria, such as *Brevundimonas* and *Pseudomonas*. Moreover, the relative abundances of the bacteria were correlated with hyperglycaemia, liver injury, and tissue inflammation. The findings of the present study could facilitate the development of effective drugs for T2DM treatment.

Materials and methods

Synthesis of GLQ.Cr

All reagents were purchased from Aladdin (Shanghai, China) and used as received. N-Bromosuccinimide (NBS; 3.916 g, 22 mmol) was dissolved in acetone (50 mL) upon slow stirring, and the solution was transferred to a dropping funnel. LUT (2.86 g, 10 mmol) was dissolved in acetone (30 mL) at room temperature (25 ℃) in the dark, and the solution was transferred to a three-necked flask, treated with benzoyl peroxide (BPO; 0.12 g, 0.5 mmol), and slowly supplemented with the NBS solution upon cooling in an ice bath. After the addition of NBS, the reaction mixture was heated to 70 °C for 12 h and concentrated *in vacuo* to obtain 6,8-bromoluteolin (3.13 g, 70.49%). A three-necked flask was charged with borax (3.81 g, 10 mmol) and 6,8-bromoluteolin (2.22 g, 5 mmol), and the reaction mixture was supplemented with 1 M aqueous NaOH to achieve a pH of 9 and stirred for 3 h to synthesize a 6,8-bromoluteolin–boric acid complex (2.2 g, 82.7%). The above complex (2.13 g, 4 mmol) was dissolved in toluene (80 mL) in a three-necked flask, and the solution was supplemented with guanidine hydrochloride (0.955 g, 10 mmol), Pd(II) acetate (0.05 g, 0.2 mmol; catalyst), 2-(Dicyclohexylphosphino)-3,6-dimethoxy-2′-4′-6′-tri-i-propyl-1,1′-biphenyl (BrettPhos; 0.21 g, 0.4 mmol; ligand), and sodium *tert*-butoxide (1.44 g, 15 mmol; alkali) under an atmosphere of N_2 and heated at 130 °C for 14 h. 6,8-guanidyl luteolin quinone (GLQ; 0.45 g, 28.27%) was obtained after deprotection with 0.1 M HCl and characterized using Fourier Transform Infrared Spectroscopy (FT-IR; NEXUS-670, Nicolet, USA) and High Resolution Mass Spectrum (HRMS; 1290–6545 Q-TOF, Agilent, USA). Besides, a three-necked flask was charged with ethanol (100 mL), GLQ (0.398 g, 1 mmol), and Cr(III) acetate (0.27 g, 1.2 mmol), and the mixture was heated at 60 °C upon stirring, treated with 1 M aqueous NaOH to achieve a pH of 9.8, and heated at 80 °C for 5 h. The resulting GLQ.Cr (0.39 g, 68.78%) was characterized using FT-IR spectroscopy, Ultraviolet–Visible Spectroscopy (UV–Vis spectrum; UV-2450, Shimadzu, Japan), and Scanning Electron Microscopy (SEM; Quanta-200, FEI, USA).

Animal experiments

Seventy healthy male Kunming mice (4 weeks old, 20 ± 3 g) purchased from Wu's Animal Centre (Fuzhou, China) were housed in a constant temperature and humidity barrier system (23 ± 2 °C) under a 12-h dark-light cycle and given *ad libitum* access to food and water. After a week, 10 mice were randomly selected as the Normal group and fed a chow diet, while the remaining 60 mice were fed with HSHF diet (58.8% standard chow, 15% sucrose, 15% lard, 1% cholesterol, 0.2% cholate, and 10% yolk) to induce diabetes [18]. Four weeks later, the 60 mice were i.p. injected with a streptozotocin (STZ) solution in 0.1 M citrate buffer (pH 4.5) at a dose of 45 mg/kg, while the mice in the Normal group were injected with the same volume of citrate buffer [19]. All mice were injected every other day for a total of three times, and fasting blood glucose (FBG) was quantified at 48 h after the last injection, with FBG levels > 11.1 mM assumed to indicate T2DM. The Kunming T2DM mice were randomly divided into six groups of 10 mice, and continued to be fed HSHF diets as well as intragastric administration of water (Model groups), GLQ, GLQ.Cr, LUT, MH, or CrY for four weeks at a doses of 100 mg/kg.d., whereas the mice in the Normal group were injected with the same volume of water. Body weight was determined using an electric balance (Shimadzu, Japan), and FBG levels were measured using a glucose meter (Omron, Japan). The day before euthanasia, all mice were subjected to the oral glucose tolerance test (OGTT) and area under the curve (AUC) test. On the following day, all mice were i.p. injected with 0.3% pentobarbital sodium solution at a dose of 50 mg/kg, and the mice were anesthetized. They were then sacrificed by cervical dislocation after blood had been collected from their eyeballs. Parts of the liver, pancreas, and caecum tissues were fixed with 10% formalin, and the remaining parts, as well as caecum contents and faeces, were rapidly frozen in liquid nitrogen and stored at −80 °C for further analysis. All mice were subjected to cervical dislocation after anaesthesia according to the ethical guidelines approved by the Animal Ethics Committee of Fujian Agriculture and Forestry University (ethical approval code FS-2019-013).

Determination of serum interleukin and HOMA insulin correlation index

Blood samples of mice were placed in plastic centrifuge tubes at 37 °C for 2 h and centrifuged at 1000*g* for 15 min to obtain serum samples. ELISA kits (Wuhan Chundu Biotechnology Co., Ltd., China) were used to quantify interleukin-6 (IL-6), interleukin-10 (IL-10) and fasting insulin (FIN) in serum according to the manufacturer's instructions. FBG was quantified using a glucose meter as previously described. Homeostatic model assessment (HOMA) insulin correlation indices were calculated as HOMA-pancreatic islet β-cell function index (HOMA-β): $20 \times FIN(mU/L)/[FBG(mmol/L) - 3.5]$, HOMA-insulin resistance index (HOMA-IRI): $FIN(mU/L) \times FBG(mmol/L)/22.5$, HOMA-insulin sensitivity index (HOMA-ISI): $[FIN(mU/L) \times FBG(mmol/L)]^{-1}$ [20].

Histopathological analysis

Liver and caecum tissues were embedded in paraffin, cut into 4-μm-thick sections using a microtome, and stained with hematoxylin and eosin, while pancreatic tissues were stained with an immunofluorescent insulin antibody (Boster Biological Technology Co., Ltd., China). The sections were observed under an optical microscope (Nikon Eclipse TE2000-U, Nikon, Japan) [21].

Analysis of serum and liver biochemical indices

Serum was prepared as described above. The liver supernatant was collected after liver tissue homogenisation in a saline solution (1:9, w/v). Biochemical indicators including total cholesterol (TC), triacylglycerol (TG), low-density lipoprotein cholesterol (LDL-C), high-density lipoprotein cholesterol (HDL-C), and glycated serum protein (GSP) were determined using an assay kit supplied by the Nanjing Jiancheng Bioengineering Institute (China) [18].

RNA-seq analysis and verification of differentially expressed genes (DEGs) in liver by qPCR

Total RNA was extracted from the livers of mice using an RNA extraction kit (Takara, Japan) and sequenced using an Illumina HiSeq 4000 system (Illumina Inc., San Diego, CA, USA), with raw data analysis performed using instruments supplied by Wekemo Tech Co., Ltd. (Shenzhen, China). Reads in the obtained samples were standardized by DESeq, and Gene Ontology (GO) and Kyoto Encyclopaedia of Genes and Genomes (KEGG) analyses were performed with $p < 0.05$ [22]. cDNA was synthesised using the PrimeScript™ RT reagent kit with gDNA Eraser (Takara, Japan). The transcription levels of fatty acid translocase, cluster of differ-

entiation 36 (Cd36), fabp fatty acid binding protein (Fabp), peroxisome proliferative activated receptor γ (Pparg), cytochrome P450 4A14 (Cyp4a14), and stearoyl-CoA desaturase (Scd) were determined using SYBR® Premix Ex Taq™ II (Takara, Japan), with the corresponding primers listed in **Table S1**. Quantitative PCR (qPCR) was conducted according to the following procedure: initial denaturation at 95 °C for 3 min; five cycles of [95 °C for 30 s, 45 °C for 20 s, and 60 °C for 30 s]; 20 cycles of [95 °C for 30 s, 55 °C for 20 s, and 72 °C for 30 s]; and a final extension at 72 °C for 5 min. The β-actin gene was used as a reference, and data were processed using the $2^{-\Delta\Delta Ct}$ method [23].

qPCR and western blotting analysis of hepatic genes

The detailed steps of qPCR are described in section 2.9. Liver proteins were obtained by homogenisation of murine liver tissues, separated on sodium dodecyl sulfate polyacrylamide gel electrophoresis gel, and transferred to polyvinylidene fluoride membranes (Sangon, Shanghai, China). The membranes were blocked with QuickBlock™ blocking buffer (Beyotime, Shanghai, China) for 40 min at 37 °C and incubated overnight with antibodies against Cd36, Fabp, Pparg, Cyp4a14, and Scd (Beyotime). Grayscale analysis was used as the quantitative analysis method for protein, using Image J densitometry software (National Institutes of Health, Bethesda, MD, USA) and the protein strips were observed using a GeneGnome XRQ Chemiluminescence Imaging System (Syngene, Cambridge, UK). The detailed steps of western blotting are referred to in our previous study [23].

Caecal microbiota analysis

Metagenomic DNA was extracted from caecum contents using a QIAamp DNA stool mini kit (Qiagen, Hilden, Germany). The primers used for PCR amplification were 341F 5′-CCTAYGGGRBGCAS CAG-3′ and 806R 5′-GGACTACNNGGGTATCTAAT-3′. The sequencing strategy corresponded to single-ended sequencing SE600, and Ion S5TMXL (Thermofisher, Waltham, MA, USA) was used as the sequencing platform. Sequencing results were analyzed as described by Ge et al [23].

Determination of short-chain fatty acids (SCFAs) in faeces

Faeces samples (0.2 g) of mice were homogenized in distilled water (2 mL) and centrifuged at 3000 *g* for 10 min to obtain supernatant, and then 50% sulfuric acid solution (150 μL) and diethyl ether (2.5 mL) were added, and the solutions centrifuged at 8000 *g* for 10 min. The organic phase was filtered through a microporous membrane (0.22 μm). The contents of short-chain fatty acids (SCFAs) (acetic, propionic, isobutyric, butyric, isovaleric, and valeric acids) in murine faeces were determined by gas chromatography (GC-2010Plus, Shimadzu, Japan), as described by Chen et al. [24].

FMT experiments

Thirty healthy male Kunming mice (4 weeks old, 20 ± 3 g) were acclimated for a week, and 10 mice were randomly selected as the Normal group, while the remaining 20 mice were fed the HSHF diet and injected with the STZ solution to induce T2DM. The Kunming T2DM mice were randomly divided into Model and Recipient groups. Before FMT, the T2DM mice of the Recipient group were gavaged with 200 μL of a broad-spectrum antibiotic solution (1 mg/mL ampicillin, 0.5 mg/mL neomycin, 0.5 mg/mL vancomycin, and 1 mg/mL metronidazole) and polyethylene glycol physiological saline solution (200 mg/mL) as water sources for three consecutive days [25]. Fresh faeces from the GLQ.Cr group were collected in sterile tubes and immediately transferred to an anaerobic workstation and treated with deoxygenated sterile water (0.2 g/mL). The mixture was homogenised and filtered through a gauze. The filtrate was centrifuged at 5000 *g* for 5 min, and the supernatant discarded, while the pellet was resuspended in deoxygenated sterile water to adjust the concentration of the faecal microbiota solution to 0.3 g/mL. The faecal microbiota solution was supplemented with glycerine (4:1, v/v) and stored at − 80 °C. When required, the faecal microbiota was transplanted daily via two-week oral gavaging (10 mL/kg.d). The measurements of Body weight, FBG, OGTT as well as other related indicators are referred to in section 2.2–2.5, and the sequencing of cecal contents is referred to in section 2.8.

Statistical analysis

All data are mean ± standard deviations (SD). One-way Analysis of Variance with Tukey's correction was used to analyse statistical significance, and the significance level was set at $p < 0.05$. The Spearman correlation p value between T2DM-related indicators and the related genes study variables were analysed using RStudio v3.5.2 (RStudio Inc., Boston, MA, USA).

Results

Syntheses and structures of GLQ.Cr

The synthesis of GLQ.Cr and the detailed mechanism of bromination with NBS are presented in Fig. 1. This bromination selectively yielded 6,8-bromoluteolin, in line with the directing effects of substituents on the benzene ring, and the C4, C5, C3′, and C4′ positions of 6,8-bromoluteolin were protected using borax. Subsequent C-N coupling [26] involved the reduction of $Pd^{II}(OAc)_2$(-BrettPhos)$_2$ followed by acetic dissociation to afford a Pd^0 species (Pd-BrettPhos) that oxidatively added the 6,8-bromoluteolin–boric acid complex to form an intermediate in equilibrium with its dimer. The displacement of Pd-bound Br by guanidine yielded an intermediate with a Pd–NH_2^+–C(=NH)NH_2 moiety, whose deprotonation followed by reductive elimination yielded the guanidinium-functionalised product and regenerated the catalytically active species. Finally, GLQ was coordinated with Cr(III) to synthesise GLQ.Cr. The characterization results of GLQ and GLQ.Cr are presented in **Fig. S1-S5**.

Effects of GLQ.Cr treatment on body weight, FBG, OGTT, AUC and serum interleukin

A flow chart of the animal experiments is presented in **Fig. S6.** At the beginning of the experiment, a significant body weight decrease compared to that of the Normal group was observed for the non-control groups ($p < 0.01$), while after 4 weeks, the body weight of the Normal group increased by 13.34%, while that of the Model group decreased by 9.3% (Fig. 2**A**). At Week 0, the FBG level of the Normal group was significantly lower than that of other groups, which indicated the successful establishment of the T2DM model (Fig. 2**B**). At 4 weeks, the FBG levels of GLQ and GLQ.Cr groups were significantly lower than those of the Model, LUT, and MH groups ($p < 0.05$), and the FBG level of the GLQ.Cr group was significantly lower than that of the CrY group ($p < 0.05$). After 0.5-h glucose gavage, the blood glucose level peaked in each treatment group and then declined (Fig. 2**C**). Compared with those of other groups, the blood glucose level of the Model group was steadily high. After 2 h, the blood glucose levels of the GLQ, GLQ.Cr, MH, and CrY groups were significantly lower than those of the Model group ($p < 0.05$). The AUC values of the Model group signif-

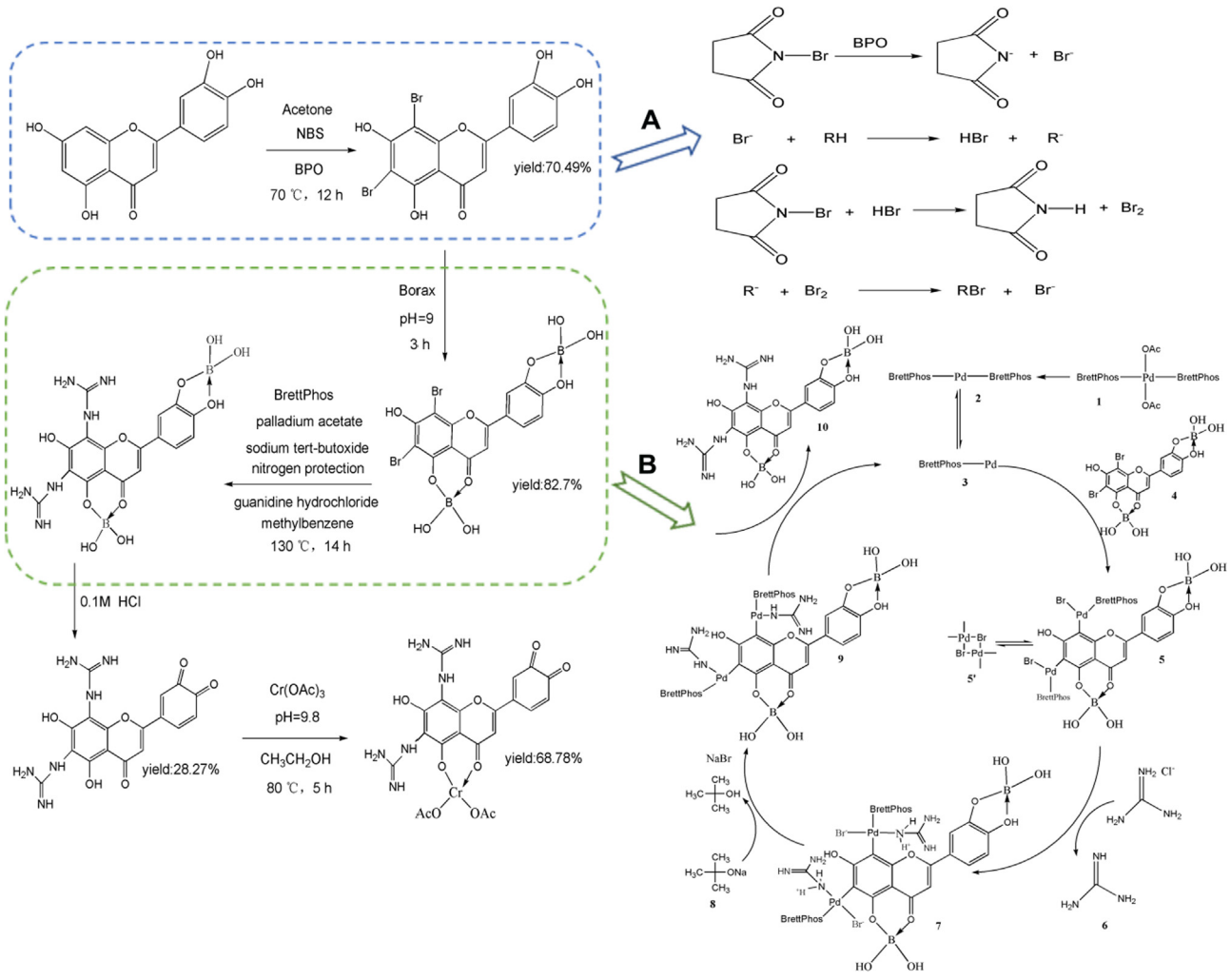

Fig. 1. The synthetic steps of GLQ.Cr. (A) The mechanism of bromine free radical reaction; (B) The mechanism of palladium acetate catalyzed C-N cross coupling reaction.

icantly exceeded those of other groups ($p < 0.01$), and the values of the GLQ and GLQ.Cr groups were significantly lower than those of the LUT and CrY groups ($p < 0.01$) (Fig. 2**D**). Herein, the serum IL-6 level in T2DM mice significantly exceeded that in the Normal group, whereas the reverse was true for IL-10 ($p < 0.01$) (Fig. 2**E & 2F**). However, after treatment with GLQ and GLQ.Cr, the levels of IL-6 and IL-10 in T2DM mice improved significantly ($p < 0.01$). In addition, the IL-10 level of the GLQ.Cr group significantly exceeded that of the GLQ group ($p < 0.05$).

Effects of GLQ.Cr on the histopathological analysis, insulin correlation index, serum, and liver biochemical indicators as well as SCFAs

The disordered hepatocytes, numerous lipid droplet vacuoles, caecal villus atrophy, and increased submucosa thickness were observed for the Model group indicating an impairment of the function of liver and caecum tissues (Fig. 2**G & 2H**). Treatment with GLQ and GLQ.Cr significantly improved liver and caecum morphology. The tissue scores of liver and caecum were presented in the **Fig. S7**. The morphology of pancreatic islet cells (blue) in the Normal group was clear, with insulin secreted in high amounts (red) and uniformly distributed (Fig. 2**I**). In contrast, a decreased insulin secretion and different insulin distribution were observed in the diabetic model group. Compared with the diabetic model group, the GLQ and GLQ.Cr groups featured higher insulin secretion, with higher amounts and a more uniform distribution of secreted insulin for the GLQ.Cr group. Compared with the Model group, GLQ and GLQ.Cr groups significantly improved the serum insulin correlation index ($p < 0.05$) (Fig. 2**J-2L**). After treatment with GLQ and GLQ.Cr for 4 weeks, the serum and liver biochemical indicators as well as SCFA contents were significantly improved ($p < 0.05$) (**Fig. S8 & S9**).

RNA-seq analysis and protein expression verification of liver

DEGs were screened and analyzed for different groups according to normalized data. A total of 1132 well-commented DEGs were screened in Normal/Model groups, among which 255 were upregulated and 877 were downregulated. Meanwhile, 434 well-commented DEGs were screened in the GLQ.Cr/Model groups, among which 161 were upregulated and 273 were downregulated (Fig. 3**A**). In addition, the volcano plots are presented in Fig. 3**B & 3C** to more directly show DEGs between different groups. In addition, we performed GO analysis on GLQ.Cr/Model groups and obtained biological process (BP), cellular component (CC), and molecular function (MF) parameters for GO enrichment histograms (Fig. 3**D**). In addition, we used the KEGG pathway display for GLQ.Cr/Model groups. As shown in Fig. 3**E**, DEGs were mainly associated with steroid biosynthesis, the PPAR signalling pathway, terpenoid backbone biosynthesis, and ECM-receptor interaction.

As shown in Fig. 4**A**, Fabp was positively correlated with serum TC, TG, GSP, LDL-C, as well as liver TC, TG, LDL-C levels, and negatively correlated with SCFA, serum HDL-C, as well as liver HDL-C

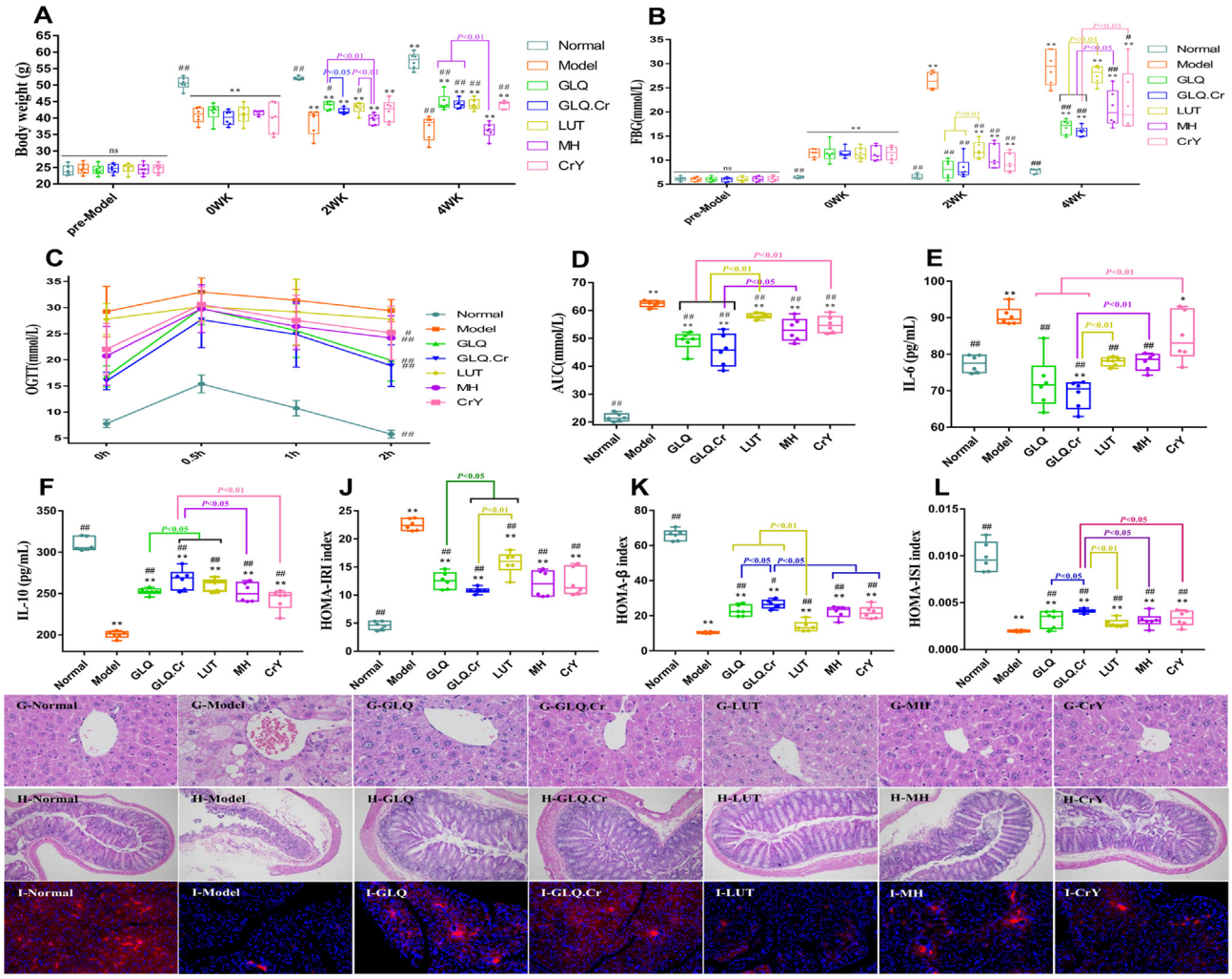

Fig. 2. Changes of mice in different groups during the experimental period. (A) Body weight; (B) FBG; (C) OGTT; (D) AUC; (E) IL-6; (F) IL-10; (G, H) Histopathological analysis of liver (400 × magnification) and caecum (100 × magnification); (I) Immunofluorescence section of pancreas tissue; (J) HOMA-IRI; (K) HOMA-β; and (L) HOMA-ISI. Normal: normal diet; Model: HSHF diet; GLQ: HSHF diet + GLQ (100 mg/kg.d); GLQ.Cr: HSHF diet + GLQ.Cr (100 mg/kg.d); LUT: HSHF diet + Luteolin (100 mg/kg.d); MH: HSHF diet + Metformin hydrochloride (100 mg/kg.d); CrY: HSHF diet + Chromium-enriched yeast (100 mg/kg.d); WK: week. Data are mean ± SD (n = 6). ns: no significant; $^{*}p < 0.05$ and $^{**}p < 0.01$ compared with the Normal group; $^{\#}p < 0.05$ and $^{\#\#}p < 0.01$ compared with the Model group.

levels. In addition, Cyp4a14 was positively correlated with serum TC and serum LDL-C levels, and negatively correlated with acetic acid, propionic acid, and liver HDL-C levels. We also filtered the parameters of $|r| > 0.75$ to draw a network graph (Fig. 4**B**). Cd36 was positively correlated with serum TG, FBG, AUC, liver LDL-C, and HOMA-IRI levels, and negatively correlated with body weight, HOMA-ISI, HOMA-β, IL-10, and valeric acid levels. Finally, to verify the accuracy of RNA-seq results, we randomly selected five genes (Cd36, Fabp, Pparg, Cyp4a14, and Scd) from the DEGs obtained by GLQ.Cr/Model group analysis for qPCR verification. The verification results (Fig. 4**C**) showed that the qPCR trends were consistent with the RNA-seq trends. Moreover, the results of both the qPCR and RNA-seq for the five genes revealed significant differences between Model and GLQ.Cr groups ($p < 0.01$). Good linear correlation was observed between qPCR and RNA-seq ($r^2 = 0.9719$) (Fig. 4**D**). Therefore, the results of qPCR verification demonstrated that RNA-seq had high accuracy and reliability. After 4 weeks, the relative mRNA transcription and protein expression levels of Cd36, Fabp, Pparg, Cyp4a14, and Scd in the diabetic model group were significantly upregulated ($p < 0.01$) compared to those in the Normal group. Treatment with GLQ and GLQ.Cr resulted in significant downregulation of relative mRNA transcription (**Fig. S10**) and protein expression levels of the five genes ($p < 0.05$) (Fig. 4**E-4G; Fig. S11 & S12**).

Effects of GLQ.Cr treatment on intestinal microbiota in caecum contents

At the phylum level, Firmicutes and Bacteroidetes were the dominant bacteria in the caecum, accounting for > 90% of the total gut microbiota (Fig. 5**A**). The Firmicutes to Bacteroidetes (F/B) ratio was significantly lower in the Normal group than in the Model group ($p < 0.01$), and the F/B ratios of GLQ and GLQ.Cr groups were significantly lower than those of the Model, MH, and CrY groups ($p < 0.05$) (Fig. 5**B**).

At the genus level, five bacterial genera with high abundance were selected for further assessment. The relative abundances of *Lactobacillus* and *Alistipes* in GLQ.Cr group significantly exceeded those in the Model group ($p < 0.05$) (Fig. 5**C-5G**), whereas the relative abundances of *Parabacteroides*, *Lachnoclostridium*, and *Desulfovibrio* were significantly lower than those of the Model group ($p < 0.05$). The relationships between intestinal microflora and T2DM-related indicators were studied using hierarchical clustering analysis (Fig. 5**H**). The relative abundance of *Alistipes* was positively

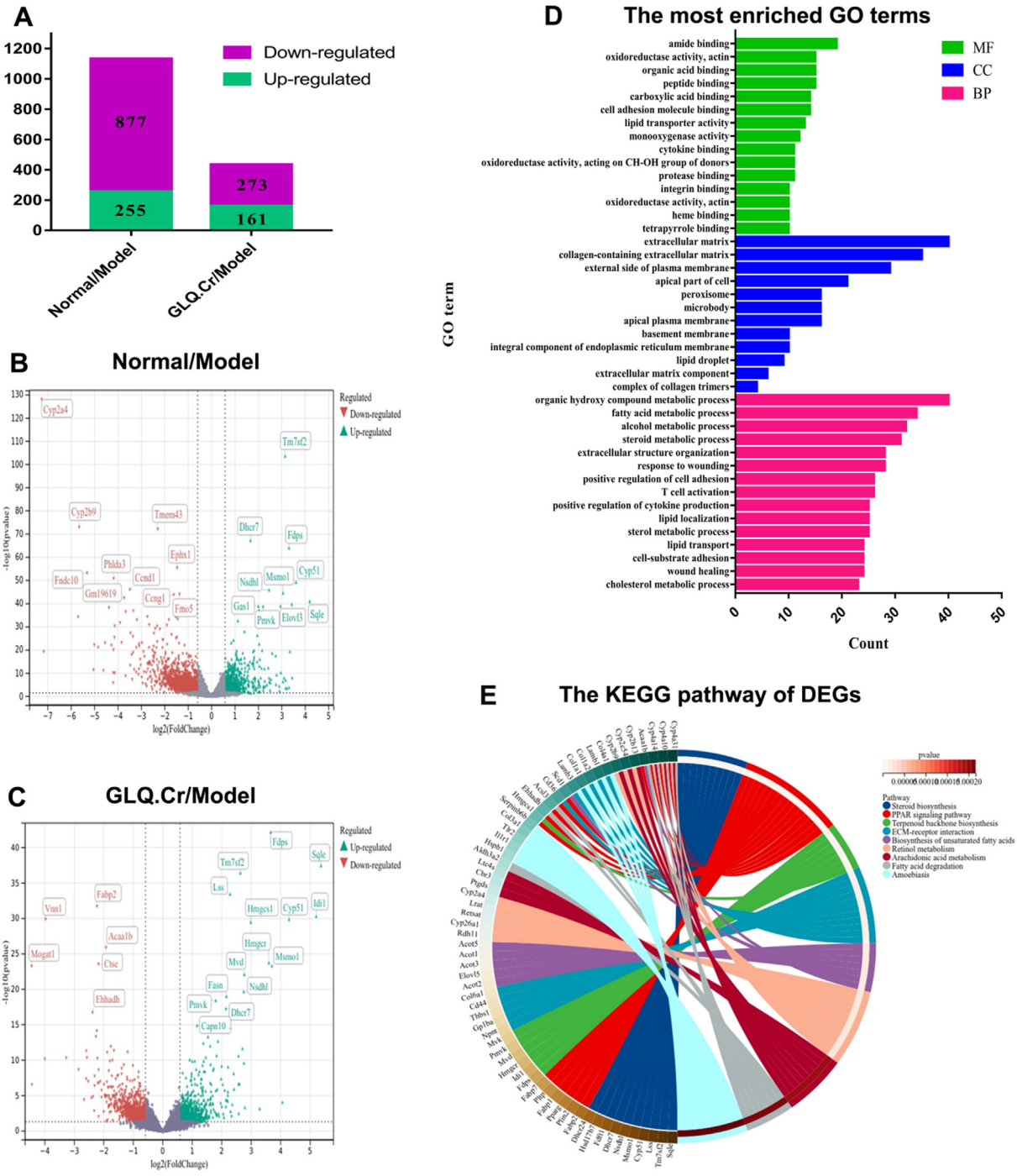

Fig. 3. Differentially expressed genes (DEGs) in the liver of mice. (A) Statistical map of DEGs between different groups; (B) Volcano map of DEGs between Normal/Model groups; (C) Volcano map of DEGs between GLQ.Cr/Model groups; (D) The GO Terms of DEGs in GLQ.Cr/Model groups; (E) The circos loop graph of KEGG pathway in GLQ.Cr/Model group.

correlated with serum HDL-C, propionic acid, acetic acid, and isovaleric acid levels, and was negatively correlated with serum LDL-C, serum GSP, and IL-6 levels. On the contrary, the relative abundance of *Lachnoclostridium* was positively correlated with serum TC, serum GSP, IL-6, and FBG levels, and was negatively correlated with liver HDL-C, IL-10, propionic acid, acetic acid, and isovaleric acid levels. The r value of anti-hyperglycemic parameters and mice caecum microbiota at the genus level are shown in **Table S2**. Furthermore, the results of network analysis (|r|>0.4) (Fig. 5**I**) showed that *Bilophila* had a strong positive correlation with serum LDL-C, liver TC, and liver TG levels.

Effects of FMT on hyperglycaemia indicators and histopathological analysis

To verify the regulatory effects of intestinal microbiota on T2DM, we first treated the Recipient group with antibiotics and polyethylene glycol physiological saline to eliminate most of the intestinal microbiota, and then transplanted the intestinal microbiota of the donor group (GLQ.Cr) into the Recipient group, using FMT (Fig. 6**A**). The body weight of T2DM mice significantly increased after two weeks of intragastric administration of faecal microbiota liquid (p < 0.01) (Fig. 6**B**). In addition, FBG, OGTT,

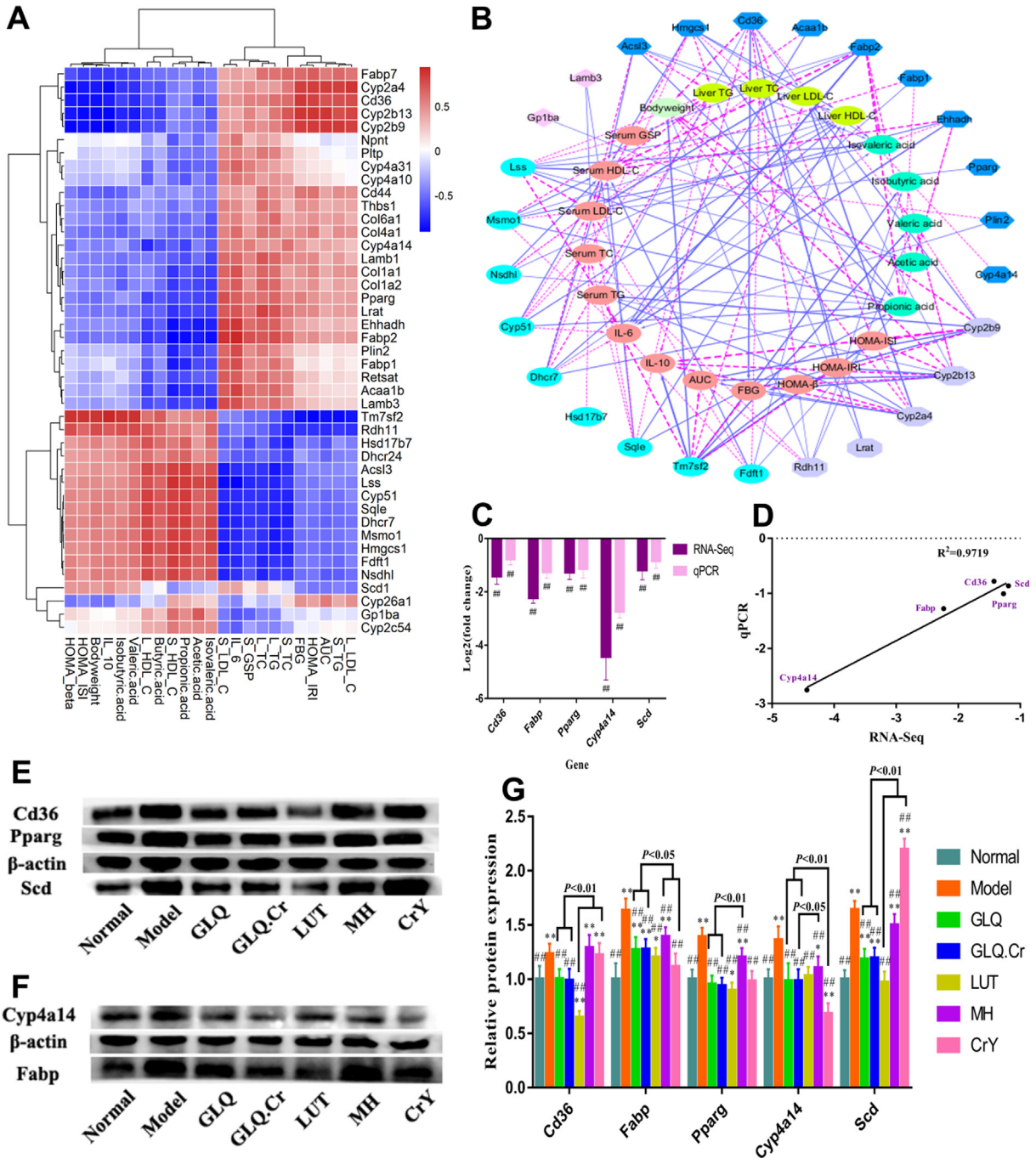

Fig. 4. (A) Hierarchical clustering analysis calculated using spearman correlation between anti-hyperglycemic correlation parameters and related genes in the four pathways of KEGG. The intensity of the colour represents the degree of association. (B) Visualization of the correlation network according to the partial correlation between the anti-hyperglycemic correlation parameters and genes. (C) qPCR verified the result of RNA-seq. (D) The linear relationship between qPCR and RNA-Seq. (E-F) Immunoblot bands of 5 proteins in each group. (G) Effects of different groups on the protein expression levels of liver genes related to glycometabolism. Quantification of band integrated density values by Image J. All the relative protein expression levels were normalized by β-actin band gray values of their corresponding groups. $^{*}p < 0.05$ and $^{**}p < 0.01$ compared with the Normal group; $^{\#}p < 0.05$ and $^{\#\#}p < 0.01$ compared with the Model group.

AUC, IL-6, and HOMA-IRI levels in the Recipient group were significantly lower than those in the diabetic model group ($p < 0.01$), while an opposite trend was observed for IL-10, HOMA-β, and HOMA-ISI levels ($p < 0.01$) (Fig. 6**C-6 J**). Moreover, compared with the Model group, the histomorphology of the liver and caecum, and the function of pancreatic islet in recipient mice were significantly improved (Fig. 6**K-6 M**). The tissue score of liver and caecum were presented in the **Fig. S13**.

Effects of FMT on serum and liver biochemical indicators as well as SCFA

Significant differences were observed between the Model and Normal groups (Fig. 7**A-7I**). Compared to those in the Model group, the serum and liver TC, TG, and LDL-C levels as well as serum GSP levels in the Recipient group were significantly decreased ($p < 0.01$), while opposite trends were observed for serum and liver

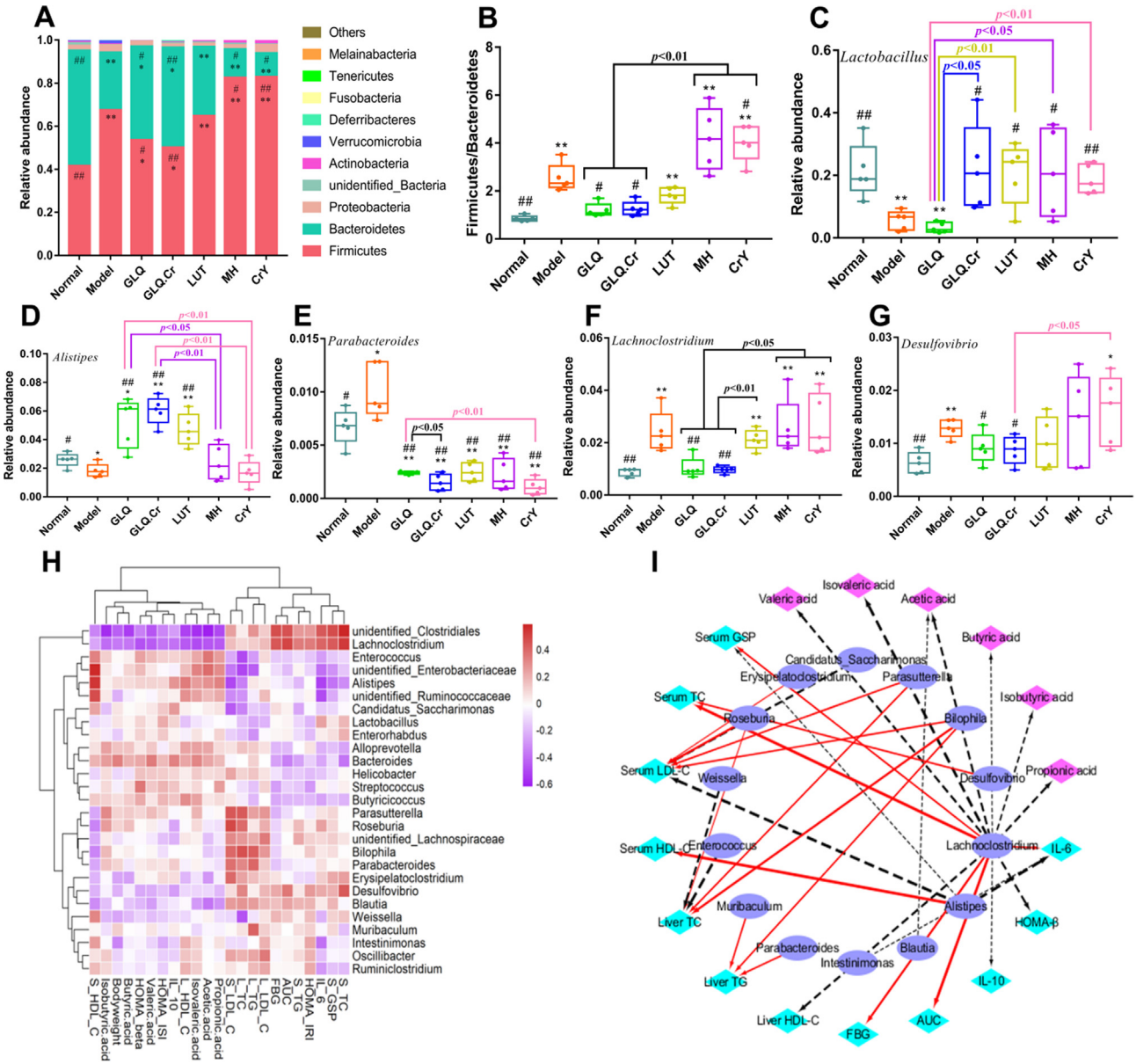

Fig. 5. Changes in the intestinal microbiota composition of mice caecum contents. Five mice were randomly selected from each group for analysis of caecal microbiota. (A) Composition of intestinal microbiota at the phylum level; (B) The ratio of Firmicutes and Bacteroidetes; (C-G) Five species of bacteria with high abundance at the genus level. $^{*}p < 0.05$ and $^{**}p < 0.01$ compared with the Normal group; $^{\#}p < 0.05$ and $^{\#\#}p < 0.01$ compared with the Model group. (H) Hierarchical clustering analysis calculated using spearman correlation of anti-hyperglycemic parameters and mice caecum microbiota at the genus level. The intensity of the colour represents the degree of association. (I) Visualization of the correlation network according to the partial correlation between the intestinal microbiota, anti-hyperglycemic correlation parameters, and SCFAs. The node colours including cyan, magenta, and SlateBlue represent the anti-hyperglycemic correlation parameters, SCFA, and intestinal microbiota genus, respectively. The solid red line and dotted black line denote positive and negative correlation, respectively. In addition, line width denotes strength of correlation. Only the significant edges are drawn in the network using the Spearman correlation test (|r|> 0.4, FDR adjusted $p < 0.01$).

HDL-C levels ($p < 0.01$). After a 2-week gavage of the Recipient group with the faecal microbiota solution, the SCFA contents in Normal and Recipient groups significantly exceeded ($p < 0.05$) those in the Model group (Fig. 7**J-7O**).

Effects of FMT on intestinal microbiota in caecum contents

Compared with the Model group, the relative abundances of Firmicutes in the Normal and Recipient groups were significantly decreased ($p < 0.05$), whereas the relative abundances of Bacteroidetes were significantly increased ($p < 0.01$) (Fig. 8**A**). The relative abundance of Proteobacteria in the Normal group was significantly lower than those in Model and Recipient groups. The Model group had a significantly higher F/B ratio than the Normal and Recipient groups ($p < 0.05$). At the phylum level, an increase in the F/B ratio enhanced the effectiveness of energy acquisition by intestinal microbiota, promoted the synthesis of fat and cholesterol, and caused diseases such as hepatic injury, insulin resistance, and other symptoms (Fig. 8**B**). At the genus level, we compared the abundance of microflora in the caecum contents of the FMT donor (GLQ.Cr) group with the Recipient group (Fig. 8**C**). Comparison of the GLQ.Cr group with the Model group revealed significant changes in the abundances of *Lactobacillus*, *Alistipes*, *Lachnoclostridium*, *Parabacteroides*, and *Desulfovibrio* ($p < 0.05$). In the case of FMT, significant differences were observed between the Recipient and Model groups in terms of *Lactobacillus*,

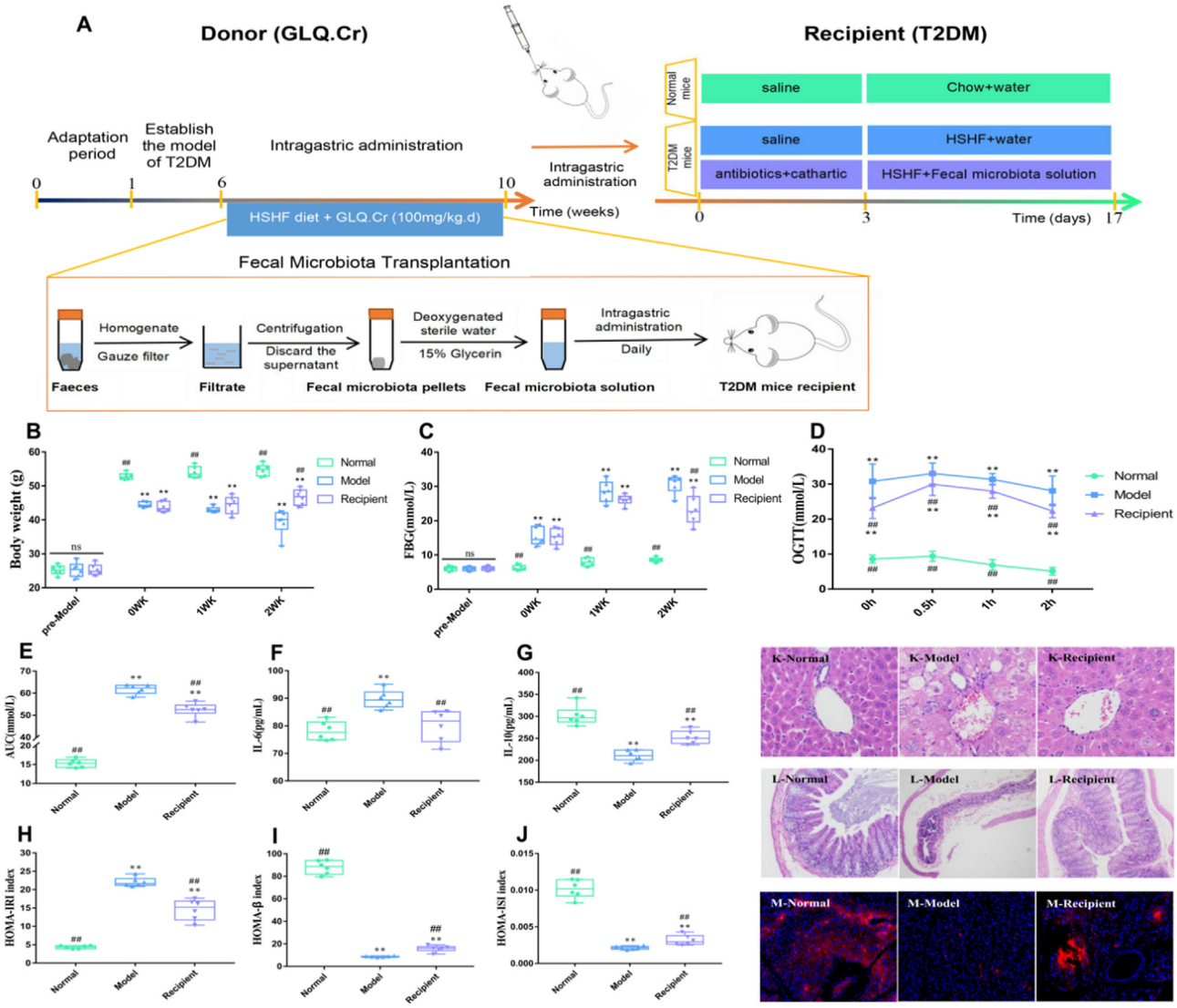

Fig. 6. Changes of mice in different groups during the FMT experimental period. (A) Schematic diagram of preparation of donor microbiota liquid and transplant of the recipient with faecal microbiota liquid; Boxplots showing change in (B) Body weight; (C) FBG; (D) OGTT; (E) AUC; (F) IL-6; (G) IL-10; (H) HOMA-IRI; (I) HOMA-β; (J) HOMA-ISI. (K, L) Histopathological analysis of liver (400 × magnification) and caecum (100 × magnification); (M) Immunofluorescence section of pancreas tissue. Normal: normal diet; Model: HSHF diet; Recipient: HSHF diet + Fecal microbiota solution (10 mL/kg.d); WK: week. Data are mean ± SD (n = 6). ns: no significant; $^{*}p < 0.05$ and $^{**}p < 0.01$ compared with the Normal group; $^{\#}p < 0.05$ and $^{\#\#}p < 0.01$ compared with the Model group.

Alloprevotella, *Alistipes*, *Bacteroides*, *Lachnoclostridium*, *Ruminiclostridium*, *Brevundimonas*, and *Pseudomonas* abundances ($p < 0.05$). Compared with those in the GLQ.Cr group, the abundances of *Lactobacillus*, *Alloprevotella*, *Alistipes*, *Bacteroides*, *Lachnoclostridium*, and *Parabacteroides* in the Recipient group were lower, with significant decreases observed for *Lactobacillus*, *Alistipes*, and *Lachnoclostridium* ($p < 0.05$). The abundances of *Desulfovibrio*, *Ruminiclostridium*, *Brevundimonas*, and *Pseudomonas* were higher in the latter group, with significant increases observed for *Brevundimonas* and *Pseudomonas* ($p < 0.01$). Finally, seven bacterial genera with high abundance were selected for further assessments. Compared with those in the Model group, the relative abundances of *Lactobacillus, Alloprevotella, Alistipes*, *Bacteroides,* and *Ruminiclostridium* in the Normal and Recipient groups were significantly increased ($p < 0.05$), while *Brevundimonas* and *Pseudomonas* were significantly decreased ($p < 0.01$) (Fig. 8**D–8 J**).

The correlations between FMT intestinal microflora and hyperglycaemia indicators are presented in Fig. 8**K**, the r value of anti-hyperglycemic parameters and FMT intestinal microflora at the genus level are shown in **Table S3**. The relative abundance of *Lactobacillus* was negatively correlated with liver TC and serum LDL-C levels, and positively correlated with liver HDL-C level. The relative abundance of *Ruminiclostridium* was negatively correlated with liver TG level and positively correlated with serum HDL-C level. The relative abundance of *Blautia* was negatively correlated with serum TC and liver TG levels, and positively correlated with isovaleric acid level. The relative abundance of *Alistipes* was positively correlated with IL-10, HOMA-β, and HOMA-ISI levels, and negatively correlated with HOMA-IRI, liver LDL-C, and FBG levels. On the contrary, the relative abundances of *Brevundimonas* and *Pseudomonas* were positively correlated with IL-6, liver TC, TG, and LDL-C levels, and negatively correlated with IL-10 and liver HDL-C levels.

Discussion

T2DM is an endocrine and metabolic disorder that is mainly characterized by elevated blood glucose levels, and is a serious

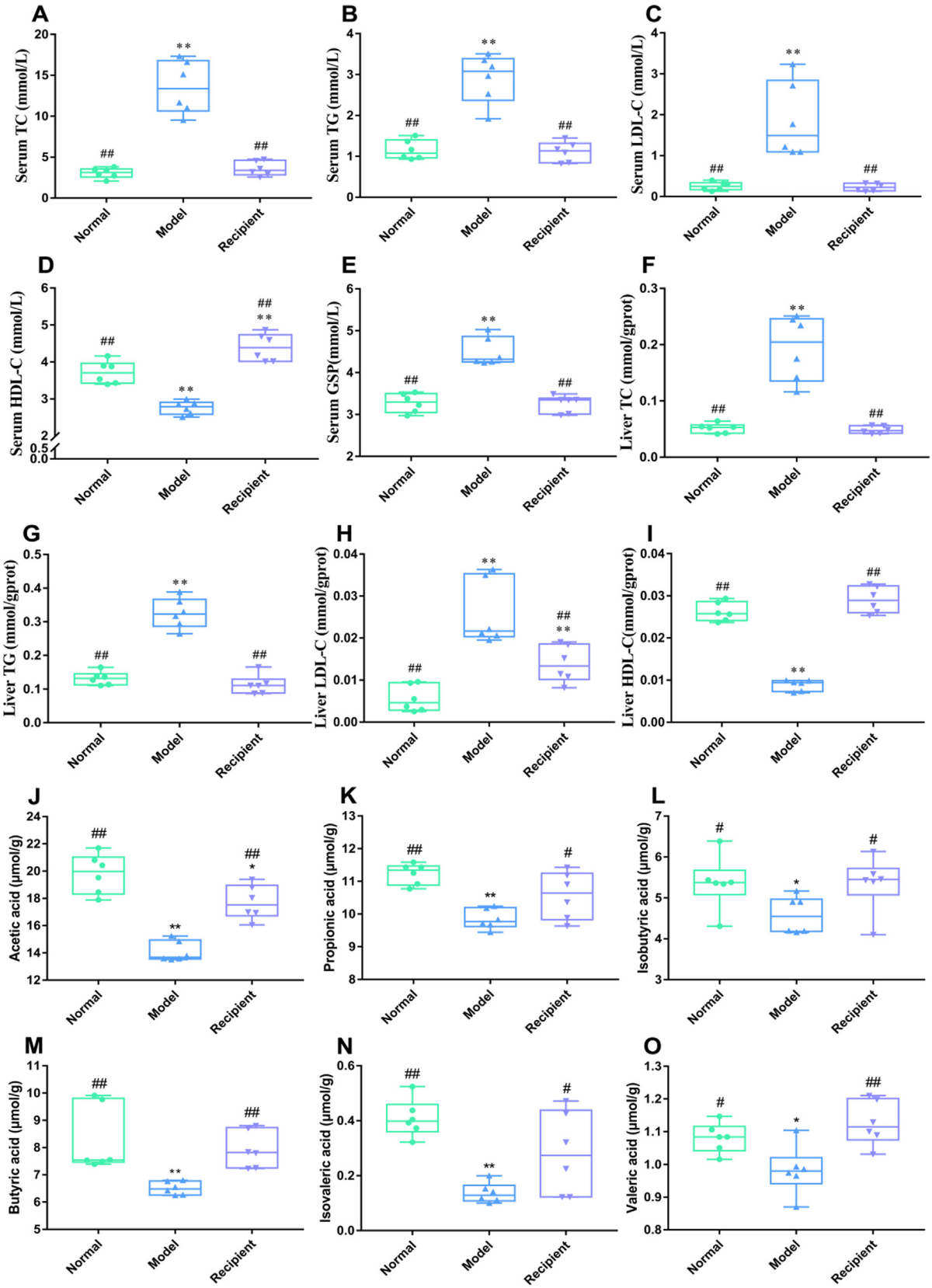

Fig. 7. Serum and liver biological indicators of mice in each group during the experimental period. (A) Serum TC; (B) Serum TG; (C) Serum LDL-C; (D) Serum HDL-C; (E) Serum GSP; (F) Liver TC; (G) Liver TG; (H) Liver LDL-C; and (I) Liver HDL-C. Effects of short chain fatty acids of faeces in each group during the experimental period. (J) Acetic acid; (K) Propionic acid; (L) Isobutyric acid; (M) Butyric acid; (N) Isovaleric acid and (O) Valeric acid. Data are mean ± SD (n = 6). $^{*}p < 0.05$ and $^{**}p < 0.01$ compared with the Normal group; $^{\#}p < 0.05$ and $^{\#\#}p < 0.01$ compared with the Model group.

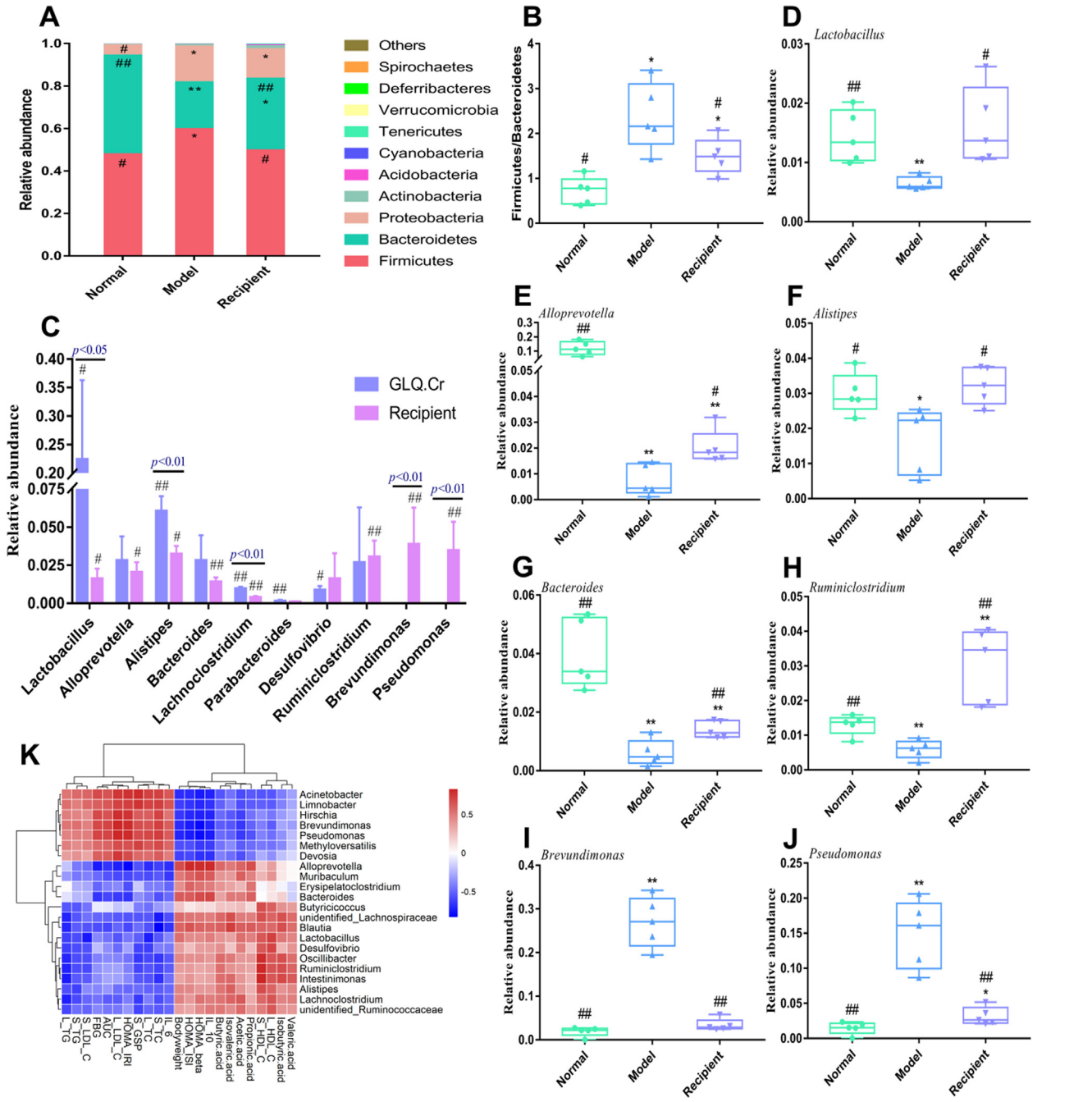

Fig. 8. Intestinal microbiota composition in mice caecum contents. Five mice were randomly selected from each group for analysis of caecal microbiota. (A) Composition of intestinal microbiota at the phylum level; (B) The ratio of Firmicutes and Bacteroidetes; (C) Abundance of microflora in cecum contents of the donor for FMT(GLQ.Cr) and recipient; (D-J) Seven species of bacteria with high abundance at the genus level; (K) Hierarchical clustering analysis calculated using spearman correlation between anti-hyperglycemic correlation parameters and FMT mice caecum microbiota at the genus level. The intensity of the colour represents the degree of association. $^{*}p < 0.05$ and $^{**}p < 0.01$ compared with the Normal group; $^{\#}p < 0.05$ and $^{\#\#}p < 0.01$ compared with the Model group.

chronic disease threatening public health. It is further associated with obesity, hepatic injury, insulin resistance, and pancreatic islet cell dysfunction [27]. Herein, GLQ.Cr was demonstrated to ameliorate the symptoms of hyperglycaemia in T2DM mice by regulating a series of related biochemical indicators and intestinal microbiota. The hypoglycaemic action mechanism of GLQ.Cr was assessed at several cellular levels i.e., RNA-seq, wherein mRNA transcription and protein expression levels of key genes were verified by qPCR and western blotting. FMT was used to transplant the faecal microbiota fluid of the donor (GLQ.Cr) group to the Recipient (T2DM) group, and the effects of blood glucose reduction and improvement of intestinal microbial communities in the Recipient group were verified.

T2DM can exhibit a series of symptoms, such as hyperglycaemia, hyperlipidaemia, and body weight reduction. High blood glucose levels hinder the absorption of energy substances, which are in turn excreted with urine to result in weight loss [21]. Four-week gavaging of GLQ or GLQ.Cr significantly increased the body weight of T2DM mice (with a better effect observed for the latter group), as these substances promoted the absorption of glucose and reduced energy loss [28]. In contrast, MH administration during T2DM treatment reduces liver glycogen consumption,

decreases the energy supply of glucose to muscle tissue, inhibits the absorption of glucose from the intestine, and ultimately leads to a decline in body weight [29]. FBG level is an important reference factor in T2DM diagnosis, reflecting the instantaneous blood glucose level. After 2-week gavaging, the hypoglycaemic effects of GLQ and GLQ.Cr were significantly superior to those of LUT, i.e., LUT did not have a significant hypoglycaemic effect (Fig. 2**B**). The FBG levels in GLQ and GLQ.Cr groups at 4 weeks were higher than those at 2 weeks, which was potentially due to drug resistance development. However, we did not dissect all the mice in the second week, as the experiments were performed according to the State Food and Drug Administration [2012] No. 107 Method for the Assessment of Assisting Blood Sugar Reduction Function (http://www.cfda.com.cn/NewsDetail.aspx?id = 53366). According to the method, the autopsy and hypoglycaemic indicator measurements are conducted after 4 weeks of intragastric administration. FBG and serum GSP levels were also investigated to monitor blood glucose levels in T2DM mice for 2–3 weeks and observe the short-term therapeutic effects of drugs. Serum GSP levels were less affected by transient fluctuations in blood glucose than FBG [30]. OGTT and AUC values were used to evaluate the capacity of pancreatic islet β-cells to regulate blood glucose concentrations [31]. GLQ and GLQ.Cr administration significantly improved serum GSP, OGTT, and AUC levels in T2DM mice.

According to the HOMA principle, in the case of an empty stomach, the relationship between blood glucose and serum insulin reflects the balance between glucose metabolism, glycogenolysis, and insulin secretion [32]. Based on the principle, we evaluated insulin resistance index, insulin sensitivity index, and function of pancreatic islet β-cells. According to the results, GLQ and GLQ.Cr significantly improved the function of pancreatic islets in T2DM mice (Fig. 2**J-2L**). The results of immunofluorescence staining indicated that treatment with GLQ or GLQ.Cr significantly increased insulin secretion in the pancreatic tissue and restored the function of the pancreas islets. The findings are consistent with the results of pancreatic function evaluation above. In addition, the restorative effect of GLQ.Cr on the pancreatic function was significantly better than that of GLQ, which indicated that the coordinated Cr(III) facilitated pancreatic tissue recovery and increased the absorption of glucose by tissues. Notably, although Cr(III) was also present in Cr-rich yeast, the FBG and AUC levels of the CrY group were significantly higher than that of the GLQ.Cr group (Fig. 2**B & 2D**), which may be due to the high molecular weight of Cr-rich yeast proteins and the difficulty of their absorption, and in turn, ability to reach the therapeutic target. High blood glucose levels in T2DM mice can further aggravate liver tissue injury, leading to changes in serum and liver-related indicators, such as TC, TG, HDL-C, and LDL-C. GLQ and GLQ.Cr significantly improved the serum and liver TC, TG, LDL-C, and HDL-C levels in T2DM mice (**Fig. S8**). Hepatic injury can slow down the rate of fatty acid decomposition and oxidation, leading to fat deposition in the liver. The spectrum of liver injury diseases is collectively referred to as NAFLD and can trigger a series of non-specific inflammations, promote the release of inflammatory cytokines, and induce the abnormal phosphorylation of insulin receptor substrate 1; at the same time, pro-inflammatory cytokines can be released into the intestinal tract to cause low-level chronic inflammation, both of which can further aggravate T2DM symptoms [33]. Treatment with GLQ and GLQ.Cr significantly improved liver and caecum morphology as well as the function of the pancreas.

As cytokines with multipotent immunomodulatory functions, IL-6 and IL-10 are produced by activated lymphocytes and are involved in immunomodulatory, inflammatory, and tumour processes. Therefore, serum IL-6 and IL-10 levels can be used to evaluate the degree of inflammation and disease development trends. Herein, the serum IL-6 level in T2DM mice significantly exceeded that in the Normal group, whereas the reverse was true for IL-10. The trends indicated that the T2DM mice presented an inflammatory response. However, after treatment with GLQ and GLQ.Cr, the levels of IL-6 and IL-10 as well as the degree of inflammation in T2DM mice significantly improved (Fig. 2**E-2F**), which is consistent with the results of histopathological analysis. In addition, the IL-10 level of the GLQ.Cr group was significantly higher than that of the GLQ group, suggesting that Cr(III) coordination had a certain anti-inflammatory effect on T2DM mice. Interestingly, treatment with CrY did not significantly decrease IL-6 level in T2DM mice, which may be due to the higher molecular weight of Cr-rich yeast proteins and, hence, their inefficient utilization by the organism. Therefore, GLQ and GLQ.Cr significantly improved the serum and hepatic biochemical indicators of T2DM mice, restored the morphology of the liver/caecum tissues and the function of the pancreas, regulated IL-6 and IL-10 levels, and alleviated the inflammation effects of T2DM on tissue function. More importantly, the effect of GLQ.Cr on inflammation in T2DM mice was significantly better than that of GLQ.

RNA-seq is an important approach of studying the level of gene transcription in a specific tissue. Herein, the number of DEGs in the Normal/Model group significantly exceeded that in the GLQ.Cr/Model group, which indicated the effectiveness of the T2DM mouse model and revealed a significant difference in gene transcriptional levels between Model and Normal mice. However, the lower number of DEGs in the GLQ.Cr/Model group indicated that GLQ.Cr significantly improved the transcriptional level of certain genes to alleviate glucose metabolism disorders in T2DM mice (Fig. 3**A**). According to the results of KEGG enrichment analysis, GLQ.Cr improved the hyperglycaemia symptoms in T2DM mice mainly by affecting the PPAR signalling pathway, which regulates the disorders of glucose/lipid metabolism, insulin secretion, and anti-inflammatory processes. To examine the accuracy of the RNA-Seq results, we selected five genes (Cd36, Fabp, Pparg, Cyp4a14, and Scd) for transcriptional level verification. Nagao et al. showed that Cd36 (a fatty acid translocase) is a key molecule that influences insulin secretion and plays a crucial role in T2DM pathogenesis [34]. The activation of Cd36 upregulates the expression of fatty acid binding protein (Fabp), which is mainly involved in the absorption and utilization of fatty acids in the gut. Overly high expression of Fabp increases the postprandial blood glucose levels, serum lipid levels, and carotid intima-media thickness, leading to vessel injury, atherosclerosis, and other diseases [35]. In addition, Fabp activity can upregulate the expression of Pparg [36], which is a therapeutic target for T2DM and closely associated with the occurrence of diabetes [37]. In addition, Pparg can simultaneously regulate Cyp4a14 and stearoyl-CoA desaturase (Scd), with Cyp4a14 mainly involved in the lipid homeostasis regulation of fatty acids [38], while Scd is a key enzyme for the generation of unsaturated fatty acids from saturated fatty acids. When the expression of Scd is upregulated, the amount of synthesized would increase to induce lipid accumulation in hepatocytes leading to the initiation of an oxidative stress response, which further triggers a series of diseases, such as inflammation, diabetes, and NAFLD [39]. Cd36, Fabp, Pparg, Cyp4a14, and Scd are genes in the PPAR signalling pathway that play important roles in regulating lipid metabolism disorders, the pancreatic function, and anti-inflammatory properties. qPCR was used to verify the mRNA transcription levels of the above genes, and the results revealed that the variation of these levels was consistent with the RNA-seq data (Fig. 4**C-4D**), indicating that the data were reliable. We also studied the mRNA transcription and protein expression levels of the five genes in the PPAR signalling pathway, revealing that GLQ.Cr could downregulate the mRNA transcription and protein expression levels of Cd36, Fabp, Pparg, Cyp4a14, and Scd in T2DM mice (Fig. 4**G & Fig. S10**). The downregulation of Cd36 and Pparg showed

that GLQ.Cr could improve the pancreatic function and hyperglycaemia symptoms in T2DM mice, which is consistent with the results of HOMA-IRI, HOMA-ISI, HOMA-β, and FBG analyses. Moreover, the downregulation of Fabp and Cyp4a14 was consistent with the downward trends of lipid metabolism–related indicators, such as TC and TG. The downregulation of Scd suggested that GLQ.Cr could relieve inflammation in T2DM mice, in line with the decrease in IL-6 levels and the increase in IL-10 levels. All of the results above confirmed that GLQ.Cr regulated the gene transcription and protein expression levels of Cd36, Fabp, Pparg, Cyp4a14, and Scd in the PPAR signalling pathway to enhance lipid homeostasis, improve pancreatic function, and reduce inflammatory response caused by oxidative stress, to achieve blood glucose regulation.

SCFAs, which mainly correspond to acetic, propionic, isobutyric, butyric, isovaleric, and valeric acids, play important roles in the regulation of metabolic processes [40]. In particular, acetic acid is absorbed into the bloodstream from the intestinal tract and acts as the main precursor of cholesterol, participates in the regulation of metabolism, and provides energy [41]. Propionic acid is mainly produced by the succinic acid pathway and is absorbed in the colon, providing energy for liver metabolism [6]. Butyric acid can promote the differentiation and maturation of pancreatic islet β-cells and improve the symptoms of glucose metabolism disorders [42]. Herein, GLQ and GLQ.Cr could significantly increase the SCFA contents in the faeces of T2DM mice (**Fig. S9**). In addition, SCFA content was closely related to intestinal microbiota community. Imbalance in gut microbiota and SCFAs can disrupt intestinal barrier function, alter the permeability of the intestinal mucosa, and promote immune inflammatory responses, thereby aggravating the inflammation of hepar and fluctuation of blood glucose levels, in addition to promoting the occurrence and development of chronic complications of T2DM [43]. At the phylum level, the F/B ratio is known to be closely related to hepatic injury, insulin resistance, and other symptoms [44]. In the present study, GLQ and GLQ.Cr alleviated hyperglycaemia by regulating the F/B ratio in T2DM mice at the phylum level. Notably, the F/B ratio in both the MH and CrY groups significantly exceeded that in the Model group, which was probably due to the increase in the concentration of glucagon-like peptide-1 and bile acids in the intestinal canal, and the resulting disorder of intestinal microbiota communities in the two groups (Fig. 5**A**). Combined with the results of caecal histopathological analysis, the above findings indicate that MH can damage the intestinal tract wall. Despite its inability to modulate intestinal microbiota, CrY could enhance the function of insulin, and thus, exert a hypoglycaemic effect [45]. Combined with the results of the evaluation of the pancreas islet function index (Fig. 2**-J-2L**), the results above confirmed that CrY facilitated recovery of pancreatic islet function in T2DM mice. At the genus level, *Lactobacillus* and *Alistipes* in the gut produce organic acids, bacteriocins, and other substances exerting anti-microbial and anti-inflammatory effects, and thus, maintain the balance of the intestinal environment [46]. However, increases in the relative abundances of *Parabacteroides*, *Lachnoclostridium*, and *Desulfovibrio* can give rise to inflammation and insulin resistance [47]. GLQ and GLQ.Cr could improve inflammation and hyperglycaemia symptoms by regulating the abundances of *Alistipes*, *Parabacteroides*, *Lachnoclostridium*, and *Desulfovibrio* at the genus level. Moreover, high abundances of *Alistipes* and low abundances of *Lachnoclostridium* decreased the serum LDL-C, GSP, and IL-6 levels and reduced serum lipid, glucose, and inflammation marker levels, ultimately improving T2DM symptoms. The result is consistent with the findings of Walsh et al. [46] and Zhang et al. [47]. Devkota et al. observed that mice fed a saturated (milk-derived) fat diet featured higher relative abundances of *Bilophila* and increased levels of TC, TG, and LDL-C [48]. This research also confirmed that *Bilophila* abundance was strongly positively correlated with TC, TG, and LDL-C levels.

The weight of T2DM mice significantly increased after 2 weeks of intragastric administration of faecal microbiota liquid, indicating that the transplanted faecal microbiota of the GLQ.Cr group could increase the absorption and utilization of glucose in tissues, reverse weight reduction, and significantly reduce blood glucose levels (Fig. 6**B-6E**). The results of pancreatic function evaluation according to the HOMA principle showed that the pancreatic function of the Recipient group recovered to a certain extent. The conclusion was confirmed by the results of the immunofluorescence analysis of the pancreatic tissue and was consistent with the results of FBG analysis (Fig. 6). The histomorphology of the liver and caecum of recipient mice significantly improved (Fig. 6**K-6L**), and the decrease in IL-6 levels and the increase in IL-10 levels (Fig. 6**F-6G**) demonstrated that the inflammation symptoms were significantly reduced. The combined effects could significantly improve the levels of TC, TG, LDL-C, and HDL-C in the serum and liver (Fig. 7). The transplantation of faecal microbiota fluid from GLQ.Cr-treated mice significantly improved the symptoms of hyperglycaemia and pancreatic function in T2DM mice, restored the histological morphology of the liver and caecum, and reduced the inflammatory responses. Furthermore, the administration of the faecal microbiota liquid of GLQ.Cr-treated mice significantly increased the abundances of *Lactobacillus*, *Alloprevotella*, *Alistipes*, and *Bacteroides,* while decreasing the abundances of *Brevundimonas* and *Pseudomonas* in the caecum of T2DM mice (Fig. 8**D-8G & 8I-8 J**). The behaviour indicated that the faecal microbiota liquid of GLQ.Cr-treated mice effectively improved the intestinal microflora communities of T2DM mice. Finally, we explored the relationship between the intestinal microbiota at the genus level and the above indicators. Increases in the relative abundances of *Lactobacillus*, *Alloprevotella*, *Alistipes*, *Bacteroides*, and *Ruminiclostridium* decreased blood glucose level and degree of inflammation, while increasing SCFA contents in faeces (Fig. 8**K**). Xiao et al. observed that *Scutellariae radix* and *Coptidis rhizoma* regulated TC, TG, LDL-C, FBG, and HDL-C levels by increasing the relative abundance of *Ruminiclostridium* in the gut [49]. The result is consistent with the strong correlation observed herein between the relative abundance of *Ruminiclostridium* and TG and HDL-C levels. In addition, Zhai et al. reported that curcumin could increase the relative abundance of *Blautia* to alleviate liver injury [50], while liver injury could directly increase the levels of TC and TG. In the present study, the relative abundance of *Blautia* was strongly correlated with TC, TG, and isovalerate levels. In addition, *Brevundimonas* and *Pseudomonas* abundances were positively correlated with IL-6, liver TC, TG, and LDL-C levels, i.e., the above microorganisms could improve liver inflammation and enhance lipid homeostasis. Yoo et al. demonstrated that *Brevundimonas* could cause immunodeficiency and hepatic cysts in the host [51], whereas Ilaiwy et al. observed that *Pseudomonas* could trigger sepsis and impair liver and intestinal tissues [52]. The findings are consistent with ours. The above results demonstrate that the faecal microbiota liquid of GLQ.Cr-treated mice can alter the intestinal microflora communities of T2DM mice, increase SCFA contents, reduce blood glucose levels, and relieve inflammation caused by oxidative stress to ameliorate T2DM symptoms. Therefore, the transplantation of faecal samples from GLQ.Cr-treated mice into T2DM mice by FMT exerted hypoglycaemic effects.

Conclusion

Our results demonstrate that treatment with GLQ.Cr could ameliorate hyperglycaemia, liver injury, tissue inflammation, and other symptoms in T2DM mice. RNA-seq analysis indicated that GLQ.Cr

corrected the abnormal glucose metabolism in T2DM mice by regulating the PPAR signalling pathway, and the key genes were verified at the transcriptional and protein expression levels. Caecal content sequencing revealed that GLQ.Cr administration could decrease blood glucose levels by regulating the communities of intestinal microbes, supporting the notion that the gut microbiota mediates the anti-hyperglycemic action in treated animal group. To confirm such hypothesis, transplantation of the faecal microbiota liquid of GLQ.Cr-treated mice into T2DM mice was carried out and the findings demonstrated a regulation of intestinal microflora communities and alleviation of the hyperglycaemia symptoms. Moreover, the transplantation provides a novel strategy for the further study of functional intestinal microflora in relation to metabolic diseases caused by T2DM, and is yet to be examined for other flavonoid analogues.

Compliance with Ethics Requirements

This article does not contain any studies with human participants performed by any of the authors. This study was approved by the ethical committee of the Fujian Agriculture and Forestry University. All subjects gave written informed consent.

CRediT authorship contribution statement

Xiaodong Ge: Conceptualization, Methodology, Data curation, Writing – original draft. **Xiaoyu He:** Conceptualization, Methodology, Investigation, Data curation. **Junwei Liu:** Conceptualization, Methodology, Formal analysis. **Feng Zeng:** Conceptualization, Methodology, Data curation. **Ligen Chen:** Methodology, Validation. **Wei Xu:** Software, Formal analysis. **Rong Shao:** Conceptualization, Investigation. **Ying Huang:** Methodology, Investigation. **Mohamed A. Farag:** Methodology, Writing – review & editing. **Esra Capanoglu:** Writing – review & editing. **Hesham R. El-Seedi:** Writing – review & editing. **Chao Zhao:** Conceptualization, Methodology, Project administration, Writing – review & editing, Funding acquisition. **Bin Liu:** Conceptualization, Methodology, Project administration, Writing – review & editing, Funding acquisition.

Declaration of Competing Interest

The authors declare that they have no known competing financial interests or personal relationships that could have appeared to influence the work reported in this paper.

Acknowledgement

This work was supported by Fujian Province Science and Technology Major Special Projects (2021NZ0101 & 2014NZ2002-1), Interdisciplinary Integration to Promote the High-Quality Development Projects of Juncao Science and Industry (XKJC-712021030), Natural Science Foundation of Fujian Province (2020J02032), and 1st Fujian 'Young Eagle Program' Youth Top Talent Program.

Appendix A. Supplementary material

Supplementary data to this article can be found online at https://doi.org/10.1016/j.jare.2022.06.003.

References

[1] van der Klaauw AA, Keogh JM, Henning E, Stephenson C, Kelway S, Trowse VM, et al. Divergent effects of central melanocortin signalling on fat and sucrose preference in humans. Nat Commun 2016;7(1). doi: https://doi.org/10.1038/ncomms13055.
[2] Zhao C, Yang C, Wai STC, Zhang Y, P. Portillo M, Paoli P, et al. Regulation of glucose metabolism by bioactive phytochemicals for the management of type 2 diabetes mellitus. Crit Rev Food Sci Nutr 2019;59(6):830–47. doi: https://doi.org/10.1080/10408398.2018.1501658.
[3] International Diabetes Federation. IDF Diabetes Atlas. 9th ed. International Diabetes Federation: Busan, Korea; 2019.
[4] Takemori H, Hamamoto A, Isogawa K, Ito M, Takagi M, Morino H, et al. Mouse model of metformininduced diarrhea. BMJ Open Diabetes Res Care 2020;8(1): e000898. doi: https://doi.org/10.1136/bmjdrc-2019-000898.
[5] Yan X, Yang C, Lin G, Chen Y, Miao S, Liu B, et al. Antidiabetic potential of green seaweed *Enteromorpha prolifera* flavonoids regulating insulin signaling pathway and gut microbiota in type 2 diabetic mice. J Food Sci 2019;84 (1):165–73. doi: https://doi.org/10.1111/1750-3841.14415.
[6] Farag MA, Abdelwareth A, Sallam IE, el Shorbagi M, Jehmlich N, Fritz-Wallace K, et al. Metabolomics reveals impact of seven functional foods on metabolic pathways in a gut microbiota model. J Adv Res 2020;23:47–59. doi: https://doi.org/10.1016/j.jare.2020.01.001.
[7] Zhao L, Zhang F, Ding X, Wu G, Lam YY, Wang X, et al. Gut bacteria selectively promoted by dietary fibers alleviate type 2 diabetes. Science 2018;359 (6380):1151–6.
[8] Rosa MM, Agustín A. The role of the gut-liver axis in metabolic dysfunction-associated fatty liver disease. Front Immunol 2021;12:. doi: https://doi.org/10.3389/fimmu.2021.660179660179.
[9] de Groot PF, Frissen MN, de Clercq NC, Nieuwdorp M. Fecal microbiota transplantation in metabolic syndrome: History, present and future. Gut Microbes 2017;8(3):253–67. doi: https://doi.org/10.1080/19490976.2017.1293224.
[10] Zhou D, Pan Q, Shen F, Cao HX, Ding WJ, Chen YW, et al. Total fecal microbiota transplantation alleviates high-fat diet-induced steatohepatitis in mice via beneficial regulation of gut microbiota. Sci Rep 2017;7(1). doi: https://doi.org/10.1038/s41598-017-01751-y.
[11] Ortega-Santos CP, Al-Nakkash L, Whisner CM. Exercise and/or genistein treatment impact gut microbiota and inflammation after 12 weeks on a high-fat, high-sugar diet in C57BL/6 mice. Nutrients 2020;12:E3410. doi: https://doi.org/10.3390/nu12113410.
[12] Agunloye OM, Oboh G. Blood glucose lowering and effect of oyster (*Pleurotus ostreatus*)-and shiitake (*Lentinus subnudus*)-supplemented diet on key enzymes linked diabetes and hypertension in streptozotocin-induced diabetic in rats. Food Frontiers 2022;3(1):161–71. doi: https://doi.org/10.1002/fft2.111.
[13] Zhao C, Lai S, Wu D, Liu D, Zou X, Ismail A, et al. miRNAs as regulators of antidiabetic effects of fucoidans. eFood 2020;1(1):2–11. doi: https://doi.org/10.2991/efood.k.190822.001.
[14] Lockwood TD. The lysosome among targets of metformin: new anti-inflammatory uses for an old drug? Expert Opin Therap Targets 2010;14 (5):467–78. doi: https://doi.org/10.1517/14728221003774135.
[15] Feng W, Liu Y, Fei F, Chen Y, Ding Y, Yan M, et al. Improvement of high-glucose and insulin resistance of chromium malate in 3T3-L1 adipocytes by glucose uptake and insulin sensitivity signaling pathways and its mechanism. RSC Adv 2019;9(1):114–27. doi: https://doi.org/10.1039/C8RA07470D.
[16] Ye H, Shen Z, Cui J, Zhu Y, Li Y, Chi Y, et al. Hypoglycemic activity and mechanism of the sulfated rhamnose polysaccharides chromium(III) complex in type 2 diabetic mice. Bioorg Chem 2019;88:102942. doi: https://doi.org/10.1016/j.bioorg.2019.102942.
[17] Pan Y-Y, Zeng F, Guo W-L, Li T-T, Jia R-B, Huang Z-R, et al. Effect of *Grifola frondosa* 95% ethanol extract on lipid metabolism and gut microbiota composition in high-fat diet-fed rats. Food Funct 2018;9(12):6268–78.
[18] Lin G, Liu X, Yan X, Liu D, Yang C, Liu B, et al. Role of green macroalgae *Enteromorpha prolifera* polyphenols in the modulation of gene expression and intestinal microflora profiles in type 2 diabetic mice. Int J Mol Sci 2019;20 (1):25. doi: https://doi.org/10.3390/ijms20010025.
[19] Zhao C, Yang C, Chen M, Lv X, Liu B, Yi L, et al. Regulatory efficacy of brown seaweed *Lessonia nigrescens* extract on the gene expression profile and intestinal microflora in type 2 diabetic mice. Mol Nutr Food Res 2018;62 (4):1700730. doi: https://doi.org/10.1002/mnfr.201700730.
[20] Wang J, Gao Y, Duan L, Wei S, Liu J, Tian L, et al. Metformin ameliorates skeletal muscle insulin resistance by inhibiting miR-21 expression in a high-fat dietary rat model. Oncotarget 2017;8(58):98029–39. doi: https://doi.org/10.18632/oncotarget.20442.
[21] El-Newary SA, Afifi SM, Aly MS, Ahmed RF, El Gendy A-N, Abd-ElGawad AM, et al. Chemical profile of *Launaea nudicaulis* ethanolic extract and its antidiabetic effect in streptozotocin-induced rats. Molecules 2021;26 (4):1000. doi: https://doi.org/10.3390/molecules26041000.
[22] Huang P, Tu B, Liao H-J, Huang F-Z, Li Z-Z, Zhu K-y, et al. Elevation of plasma tRNA fragments as a promising biomarker for liver fibrosis in nonalcoholic fatty liver disease. Sci Rep 2021;11(1). doi: https://doi.org/10.1038/s41598-021-85421-0.
[23] Ge X, Wang C, Chen H, Liu T, Chen L, Huang Y, et al. Luteolin cooperated with metformin hydrochloride alleviates lipid metabolism disorders and optimizes intestinal flora compositions of high-fat diet mice. Food Funct 2020;11 (11):10033–46.
[24] Chen R, Xu Y, Wu P, Zhou H, Lasanajak Yi, Fang Y, et al. Transplantation of fecal microbiota rich in short chain fatty acids and butyric acid treat cerebral ischemic stroke by regulating gut microbiota. Pharmacol Res 2019;148:104403. doi: https://doi.org/10.1016/j.phrs.2019.104403.
[25] Bárcena C, Valdés-Mas R, Mayoral P, Garabaya C, Durand S, Rodríguez F, et al. Healthspan and lifespan extension by fecal microbiota transplantation into

progeroid mice. Nat Med 2019;25(8):1234–42. doi: https://doi.org/10.1038/s41591-019-0504-5.
[26] Gioria E, del Pozo J, Martínez-Ilarduya JM, Espinet P. Promoting difficult carbon–carbon couplings: which ligand does best? Angewandte Chemie-International Edition 2016;128(42):13470–4. doi: https://doi.org/10.1002/ange.201607089.
[27] Ouyang Y, Liu D, Zhang L, Li X, Chen X, Zhao C. Green alga *Enteromorpha prolifera* oligosaccharide ameliorates ageing and hyperglycemia through gut-brain axis in age-matched diabetic mice. Mol Nutr Food Res 2022;66(4):. doi: https://doi.org/10.1002/mnfr.202270011e2100564.
[28] Luo Z, Fu C, Li T, Gao Q, Miao D, Xu J, et al. Hypoglycemic effects of Licochalcone A on the streptozotocin-induced diabetic mice and its mechanism study. J Agric Food Chem 2021;69(8):2444–56. doi: https://doi.org/10.1021/acs.jafc.0c0763010.1021/acs.jafc.0c07630.s001.
[29] Yanovski JA, Krakoff J, Salaita CG, McDuffie JR, Kozlosky M, Sebring NG, et al. Effects of metformin on body weight and body composition in obese insulin-resistant children a randomized clinical trial. Diabetes 2011;60(2):477–85. doi: https://doi.org/10.2337/db10-1185.
[30] Ford ES, Wheaton AG, Chapman DP, Li CY, Perry GS, Croft JB. Associations between self-reported sleep duration and sleeping disorder with concentrations of fasting and 2-h glucose, insulin, and glycosylated hemoglobin among adults without diagnosed diabetes. J Diabetes 2014;6:338–50. doi: https://doi.org/10.1111/1753-0407.12101.
[31] Bartoli E, Fra GP, Schianca GPC. The oral glucose tolerance test(OGTT) revisited. Eur J Intern Med 2011;22(1):8–12. doi: https://doi.org/10.1016/j.ejim.2010.07.008.
[32] Wallace TM, Levy JC, Matthews DR. Use and abuse of HOMA modeling. Diabetes Care 2004;27:1487–95. doi: https://doi.org/10.2337/diacare.27.6.1487.
[33] Galle-Treger L, Sankaranarayanan I, Hurrell BP, Howard E, Lo R, Maazi H, et al. Costimulation of type-2 innate lymphoid cells by GITR promotes effector function and ameliorates type 2 diabetes. Nat Commun 2019;10(1). doi: https://doi.org/10.1038/s41467-019-08449-x.
[34] Nagao M, Esguerra JLS, Asai A, Ofori JK, Edlund A, Wendt A, et al. Potential protection against type 2 diabetes in obesity through lower CD36 expression and improved exocytosis in β-cells. Diabetes 2020;69(6):1193–205. doi: https://doi.org/10.2337/db19-0944.
[35] Wanby P, Palmquist P, Ryden I, Brattstrom L, Carlsson M. The FABP2 gene polymorphism in cerebrovascular disease. Acta Neurol Scand 2004;110(6):355–60. doi: https://doi.org/10.1111/j.1600-0404.2004.00335.x.
[36] Tan N-S, Shaw NS, Vinckenbosch N, Liu P, Yasmin R, Desvergne Béatrice, et al. Selective cooperation between fatty acid binding proteins and peroxisome proliferator-activated receptors in regulating transcription. Mol Cell Biol 2002;22(17):6318. doi: https://doi.org/10.1128/MCB.22.17.6318.2002.
[37] Jiang C, Liu SH, Cao YW, Shan HP. High glucose induces autophagy through PPAR. PPAR Research 2018;2018:8512745. doi: https://doi.org/10.1155/2018/8512745.
[38] Lukaszewicz KM, Lombard JH. Role of the CYP4A/20-HETE pathway in vascular dysfunction of the Dahl salt-sensitive rat. Clin Sci 2013;124:695–700. doi: https://doi.org/10.1042/CS20120483.
[39] Li Z, Lu S, Cui K, Shafique L, Rehman Su, Luo C, et al. Fatty acid biosynthesis and transcriptional regulation of stearoyl-CoA desaturase 1 (SCD1) in buffalo milk. BMC Genet 2020;21(1). doi: https://doi.org/10.1186/s12863-020-0829-6.
[40] Huang L, Thonusin C, Chattipakorn N, Chattipakorn SC. Impacts of gut microbiota on gestational diabetes mellitus: a comprehensive review. Eur J Nutr 2021;60(5):2343–60. doi: https://doi.org/10.1007/s00394-021-02483-6.
[41] Wen Li, Wong FS. Dietary short-chain fatty acids protect against type 1 diabetes. Nat Immunol 2017;18(5):484–6. doi: https://doi.org/10.1038/ni.3730.
[42] Weitkunat K, Stuhlmann C, Postel A, Rumberger S, Fankhänel M, Woting A, et al. Short-chain fatty acids and inulin, but not guar gum, prevent diet-induced obesity and insulin resistance through differential mechanisms in mice. Sci Rep 2017;7(1). doi: https://doi.org/10.1038/s41598-017-06447-x.
[43] Pascale A, Marchesi N, Govoni S, Coppola A, Gazzaruso C. The role of gut microbiota in obesity, diabetes mellitus, and effect of metformin: new insights into old diseases. Curr Opin Pharmacol 2019;49:1–5. doi: https://doi.org/10.1016/j.coph.2019.03.011.
[44] Gao X, Du L, Randell E, Zhang H, Li K, Li D. Effect of different phosphatidylcholines on high fat diet-induced insulin resistance in mice. Food Funct 2021;12(4):1516–28.
[45] Elseweidy MM, Amin RS, Atteia HH, Aly MA. Nigella sativa oil and chromium picolinate ameliorate fructose-induced hyperinsulinemia by enhancing insulin signaling and suppressing insulin-degrading enzyme in male rats. Biol Trace Elem Res 2018;184(1):119–26. doi: https://doi.org/10.1007/s12011-017-1167-z.
[46] Walsh CJ, Healy S, O'Toole PW, Murphy EF, Cotter PD. The probiotic *L. casei* LC-XCAL™ improves metabolic health in a diet-induced obesity mouse model without altering the microbiome. Gut Microbes 2020;12:1–17. doi: https://doi.org/10.1080/19490976.2020.1747330.
[47] Zhang L-Y, Zhou T, Zhang Y-M, Xu X-M, Li Y-Y, Wei K-X, et al. Guiqi Baizhu decoction alleviates radiation inflammation in rats by modulating the composition of the gut microbiota. Evidence-based Complement Altern Med 2020;2020:1–13. doi: https://doi.org/10.1155/2020/9017854.
[48] Devkota S, Chang EB. Interactions between diet, bile acid metabolism, gut microbiota, and inflammatory bowel diseases. Dig Dis 2015;33(3):351–6. doi: https://doi.org/10.1159/000371687.
[49] Xiao S, Liu C, Chen M, Zou J, Zhang Z, Cui X, et al. Scutellariae radix and coptidis rhizoma ameliorate glycolipid metabolism of type 2 diabetic rats by modulating gut microbiota and its metabolites. Appl Microbiol Biotechnol 2020;104(1):303–17. doi: https://doi.org/10.1007/s00253-019-10174-w.
[50] Zhai SS, Ruan D, Zhu YW, Li MC, Ye H, Wang WC, et al. Protective effect of curcumin on ochratoxin A–induced liver oxidative injury in duck is mediated by modulating lipid metabolism and the intestinal microbiota. Poult Sci 2020;99(2):1124–34. doi: https://doi.org/10.1016/j.psj.2019.10.041.
[51] Yoo SH, Kim MJ, Roh KH, Kim SH, Park DW, Sohn JW, et al. Liver abscess caused by *Brevundimonas vesicularis* in an immunocompetent patient. J Med Microbiol 2012;61(10):1476–9. doi: https://doi.org/10.1099/jmm.0.045120-0.
[52] Ilaiwy A, ten Have GAM, Bain JR, Muehlbauer MJ, O'Neal SK, Berthiaume JM, et al. Identification of metabolic changes in ileum, jejunum, skeletal muscle, liver, and lung in a continuous I.V. *Pseudomonas aeruginosa* model of sepsis using nontargeted metabolomics analysis. The American Journal of Pathology 2019;189(9):1797–813. doi: https://doi.org/10.1016/j.ajpath.2019.05.021.